

Two-component GW calculations: Cubic scaling implementation and comparison of vertex corrected and partially self-consistent GW variants

Arno Förster,^{*,†} Erik van Lenthe,^{*,‡} Edoardo Spadetto,[‡] and Lucas Visscher[†]

[†]*Theoretical Chemistry, Vrije Universiteit, De Boelelaan 1083, NL-1081 HV, Amsterdam, The Netherlands*

[‡]*Software for Chemistry and Materials NV, NL, 1081HV, Amsterdam, The Netherlands*

E-mail: a.t.l.foerster@vu.nl; vanlenthe@scm.com

Abstract

We report an all-electron, atomic orbital (AO) based, two-component (2C) implementation of the GW approximation (GWA) for closed-shell molecules. Our algorithm is based on the space-time formulation of the GWA and uses analytical continuation of the self-energy, and pair-atomic density fitting (PADF) to switch between AO and auxiliary basis. By calculating the dynamical contribution to the GW self-energy at a quasi-one-component level, our 2C GW algorithm is only about a factor of two to three slower than in the scalar relativistic case. Additionally, we present a 2C implementation of the simplest vertex correction to the self-energy, the statically screened $G3W2$ correction. Comparison of first ionization potentials of a set of 67 molecules with heavy elements (a subset of the SOC81 set) calculated with our implementation against results from the WEST code reveals mean absolute deviations of around

70 meV for $G_0W_0@PBE$ and $G_0W_0@PBE0$. These are most likely due to technical differences in both implementations, most notably the use of different basis sets, pseudopotential approximations, different treatment of the frequency dependency of the self-energy and the choice of the 2C-Hamiltonian. However, how much each of these differences contribute to the observed discrepancies is unclear at the moment. Finally, we assess the performance of some (partially self-consistent) variants of the GWA for the calculation of first IPs by comparison to vertical experimental reference values. G_0W_0PBE0 (25 % exact exchange) and G_0W_0BHLYP (50 % exact exchange) perform best with mean absolute deviations (MAD) of about 200 meV. Explicit treatment of spin-orbit effects at the 2C level is crucial for systematic agreement with experiment. On the other hand eigenvalue-only self-consistent GW (ev GW) and quasi-particle self-consistent GW (qs GW) significantly overestimate the IPs. Perturbative G_3W_2 corrections increase the IPs and therefore improve the agreement with experiment in cases where G_0W_0 alone underestimates the IPs. With a MAD of only 140 meV, 2C- $G_0W_0PBE0 + G_3W_2$ is in best agreement with the experimental reference values.

1 Introduction

Due to its favorable price-to-performance ratio, the GW approximation (GWA)^{1,2} (G : single-particle Green’s function, W : screened electron-electron interaction) is one of the most popular methods for the calculation of charged excitations in finite systems.^{3,4} Over the last decade, the GWA has been implemented into a large number of electronic structure codes^{5–20} and GW implementations for massively parallel architectures,^{17,21–24} low-order scaling implementations,^{15,16,18,19,25} effectively linear scaling stochastic formulations,^{26,27} fragment-based approaches^{28–31} or embedding techniques^{32–34} have enabled applications of the GW method to large biomolecules,^{16,35} nanostructures^{24,31,36} or interfaces.²⁴

A large numbers of studies has by now contributed to a thorough understanding of the impact of technical aspects of these implementations, like the choice of single-particle

basis, pseudopotential (PP) approximations, or frequency treatment,^{16,37-41} as well as the performance of various *GW* approaches for the first ionization potentials (IP) and electron affinities (EA) of weakly correlated organic molecules.⁴²⁻⁴⁹ More recently, the GWA has also been benchmarked for core excitations⁵⁰⁻⁵⁴ and strongly correlated systems like open-shell molecules⁵⁵ or transition metal compounds with partially filled *3d* shells.⁵⁶⁻⁶² Fully self-consistent *GW* (sc*GW*) calculations are relatively expensive, technically demanding, and not necessarily very accurate for the calculation of IPs and EAs.^{43,46,48} Instead, the much cheaper perturbative G_0W_0 approach^{63,64} or its eigenvalue-only self-consistent extension (ev*GW*) are typically the method of choice. Despite their often excellent accuracy, these methods fail when the KS orbitals for which the *GW* corrections are evaluated are qualitatively wrong.^{35,44,46} In the quasi-particle self-consistent *GW* method (qs*GW*),⁶⁵⁻⁶⁷ the frequency dependent and non-Hermitian *GW* self-energy is mapped self-consistently to an effective static and Hermitian non-local potential which is a functional of the non-interacting single-particle Green’s function. Therefore, the results are strictly independent of the KS density functional which is used as starting-point for the calculation.^{16,35} The available benchmark data suggest that for molecules qs*GW* is at least as accurate as G_0W_0 .^{20,49,68}

Less is known about the accuracy of the GWA for molecules containing heavier elements. One reason for this is that for those systems only a limited number of accurate first-principle results are available.^{69,70} Another reason is that comparison to experimental data is complicated by spin-orbit coupling (SOC) whose explicit treatment requires to implement the GWA in a 2-component (2C) framework. While Aryasetiawan and coworkers have generalized Hedin’s equation to spin-dependent interactions^{71,72} more than a decade ago, only a few 2C implementations of the GWA for molecules have been realized so far.⁷³⁻⁷⁷ The probably most systematic study of SOC effects in molecules has been performed by Scherpelz and Govoni⁷⁴ who have compiled a set of 81 molecules containing heavy elements (referred to as SOC81 in the following).⁷⁴ They performed two-component (2C) $GW@PBE$ ⁷⁸ and $GW@PBE0$ ^{79,80} calculations for this set using the WEST code^{21,24} and found that SOC

can shift scalar relativistic (1C) first ionization potentials by up to 400 meV for molecules containing iodine.⁷⁴ Interestingly, they observed that the 1C results were often closer to experiment than the 2C ones. Also, the fact that $GW@PBE$ and $GW@PBE0$ are not necessarily very accurate for molecules^{46,48,81,82} suggests that the good performance of those methods for these systems might at least partially be due to fortuitous error cancellation. The accuracy of G_0W_0 calculations based on starting points with a higher fraction of exact exchange has however not been systematically investigated for molecules containing heavy elements. Also, little is known about the performance of partially self-consistent approaches.

In efforts to improve over the GW approximation, also the role of higher order terms in the expansion of the electronic self-energy in terms of W (vertex corrections), has been assessed over the last years for small and medium molecules.^{45,49,81,83–88} The available results suggest that they generally fail to improve consistently over the best available GW variants when they are combined with QP approximations.^{49,89,90} However, they can remove some of the starting point dependence of G_0W_0 ^{81,87} and often tremendously improve the description of electron affinities.^{84,91} With the exception of one recent study which focused on first-row transition metal oxides,⁸⁷ the available benchmark results are limited to charged valence excitations in mostly organic molecules. It is not known how these methods perform for molecules containing heavier elements, where electron correlation effects and screening effects might be stronger.

In this work, we address some of these open questions. We present systematic benchmarks of 2C-GWA at different levels of self-consistency, ranging from G_0W_0 to $qsGW$. We also investigate the effect of the statically screened $G3W2$ term⁴⁹ on the QP energies in a 2C framework. Our calculations are performed using a newly developed 2C (qs) GW implementation, a generalization of our atomic orbital based $qsGW$ and G_0W_0 algorithms.^{15,16} Our 2C implementation retains the same favorable scaling with system size and increases the prefactor of the calculations by only a factor of two compared to the 1C case. This relatively small increase in computational effort is achieved by calculating the dynamical contributions

to the electron self-energy at a quasi-one-component level. Therefore, our new implementation also allows us to describe SOC effects in large molecules. All other quantities, including the polarizability, are treated at the full 2C level without any further approximations.

The remainder of this paper is organized as follows: In section 2, we review the 2C- GW working equations and give a detailed overview of our implementation. After describing the details of our calculations in section 3, we report the results of our detailed benchmark calculations in section 2: First, to assess the influence of the different technical parameters in both implementations, we compare $G_0W_0@PBE0$ IPs for SOC81 to the ones from Scherpelz and Govoni.⁷⁴ We then use our new implementation to calculate the first ionization potentials of the molecules in the SOC81 database using some of the most accurate available GW approaches: qs GW , eigenvalue-only self-consistent GW (ev GW), eigenvalue-only self-consistent GW with fixed screened interaction after the first iteration (ev GW_0), and G_0W_0 based on hybrid starting points with different fractions of exact exchange. Finally, section 5 summarizes and concludes this work.

2 Theory

GW approximation and $G3W2$ correction

The central object of this work is the $GW + G3W2$ self-energy,

$$\Sigma^{GW+G3W2}(1, 2) = \Sigma_H(1, 2) + \Sigma^{GW}(1, 2) + \Sigma^{G3W2}(1, 2) . \quad (1)$$

Here,

$$\Sigma_H(1, 2) = v_H(1)\delta(1, 2) = -i\delta(1, 2) \int d3 v_c(1, 3)G(3, 3^+) , \quad (2)$$

with the Hartree-potential v_H ,

$$\Sigma^{GW}(1, 2) = iG(1, 2)W(1, 2) \quad (3)$$

and

$$\Sigma^{G^3W^2}(1, 2) = - \int d3d4 G(1, 3)W(1, 4)G(3, 4)G(4, 2)W(3, 2) . \quad (4)$$

Space, spin, and imaginary time indices are collected as $1 = (\mathbf{r}_1, \sigma_1, i\tau_1)$. W is the screened Coulomb interaction which is obtained by the Dyson equation

$$W(1, 2) = W^{(0)}(1, 2) + \int d3d4 W^{(0)}(1, 3)P^{(0)}(3, 4)W(4, 2) . \quad (5)$$

Here,

$$W^{(0)}(1, 2) = v_c(\mathbf{r}_1, \mathbf{r}_2)\delta_{\sigma, \sigma'}\delta(t_1 - t_2) , \quad (6)$$

is the bare Coulomb interaction and $P^{(0)}$ is the polarizability in the random phase approximation (RPA),

$$P^{(0)}(1, 2) = -iG(1, 2)G(2, 1) . \quad (7)$$

Finally, G is the interacting single-particle Green's function which is connected to its non-interacting counterpart $G^{(0)}$ by a Dyson equation with the electronic self-energy (1) as its kernel,

$$G(1, 2) = G^{(0)}(1, 2) + \int d3d4 G^{(0)}(1, 3)\Sigma(3, 4)G(4, 2) . \quad (8)$$

If necessary, one can transform all quantities to imaginary frequency using the Laplace transform⁹²

$$f(i\omega) = -i \int d\tau F(i\tau)e^{i\omega\tau} . \quad (9)$$

The self-consistent solution of eqs. (3), (5), (7) and (8) is referred to as GW approximation.

Typically, (8) is approximated. To this end, one defines an auxiliary Green's function $G^{(s)}$ which is related to $G^{(0)}$ by

$$G^{(s)} = G^{(0)}(1, 2) + \int d3d4 G^{(0)}(1, 3)v_{Hxc}(3, 4)G^{(s)}(4, 2) , \quad (10)$$

where v_{Hxc} is a (potentially local) generalized Kohn-Sham⁹³⁻⁹⁵ Hartree-exchange-correlation

potential. G is then obtained from $G^{(s)}$ by

$$G(1,2) = G^{(s)}(1,2) + \int d3d4 G^{(s)}(1,3) [\Sigma_{Hxc}(3,4) - v_{Hxc}(3,4)] G(4,2) . \quad (11)$$

In the basis of molecular orbitals (MO) $\{\phi_k\}$, $G^{(s)}$ is diagonal,

$$G_{pp'}^{(s)} = \Theta(i\tau) G_{pp'}^>(i\tau) - \Theta(-i\tau) G_{pp'}^<(i\tau) , \quad (12)$$

with greater and lesser propagators being defined as

$$G_{pp'}^>(i\tau) = -i\Theta(\epsilon_p) e^{-\epsilon_p \tau} \quad (13)$$

and

$$G_{pp'}^<(i\tau) = -i\Theta(-\epsilon_p) e^{-\epsilon_p \tau} . \quad (14)$$

Here, it is understood that all QP energies ϵ_k and KS eigenvalues ϵ_k^{KS} are measured relative to the chemical potential μ which we place in the middle of the HOMO-LUMO gap. Θ is the Heaviside step-function and $p, q, r, s \dots$ denote spinors. Under the assumption that the KS eigenstates are a good approximation to the GW eigenstates, the off-diagonal elements of the operator $\Sigma_{Hxc} - v_{Hxc}$ in (11) can be neglected. This leads to

$$[\Sigma_{xc}]_{pp}(\epsilon_p) - [v_{xc}]_{pp} = \epsilon_p - \epsilon_p^{KS} , \quad (15)$$

Solving this equation as a perturbative correction is referred to as G_0W_0 , while in $evGW$, eqs. (3), (5), (7) and (15) are solved self-consistently instead. Splitting the operator $\Sigma_{Hxc} - v_{Hxc}$ in (11) into Hermitian and anti-Hermitian part and discarding the latter one, the solution of (11) can be restricted to its QP part only.⁹⁶⁻⁹⁹ Restricting the self-energy further

to its static limit, a single-particle problem similar to the KS equations is obtained,

$$\sum_q \left\{ [\Sigma_{Hxc}^H]_{pq} - [v_{Hxc}]_{pq} \right\} \phi_q(\mathbf{r}) = (\epsilon_p - \epsilon_p^{KS}) \phi_p(\mathbf{r}), \quad (16)$$

where $\Sigma^H = \frac{1}{2} (\Sigma + \Sigma^\dagger)$ denotes the Hermitian part of the self-energy. Solving eqs. (3), (5), (7) and (16) self-consistently is referred to as the qsGW⁶⁵⁻⁶⁷ approximation.¹⁰⁰ There are many possible ways to construct the qsGW Hamiltonian.^{67,101-104} In our implementation, we use the expression

$$[\Sigma^{(GW)}(\{\epsilon_n\})]_{pq} = \begin{cases} [\Sigma^{(GW)}(\epsilon_p)]_{pq} & p = q \\ [\Sigma^{(GW)}(\tilde{\epsilon})]_{pq} & \text{else} . \end{cases} \quad (17)$$

with $\tilde{\epsilon} = 0$. If, as in our implementation,¹⁶ the self-energy on the real frequency axis is calculated via analytical continuation (AC), eq. (17) is numerically more stable^{16,105} than constructions of the qsGW Hamiltonian in which also the off-diagonal elements are evaluated at the QP energies.^{10,67}

Kramers-restricted two-component formalism

Recently, an 2C implementation of the GWA for Kramers-unrestricted systems has been implemented by Holzer with $\mathcal{O}(N^4)$ scaling with system size.⁷⁷ In this work we will focus on application to closed-shell molecules with no internal or external magnetic fields. This allows us to simplify the treatment considerably as it possible to define a Kramers-restricted set of spinors in which pairs of spinors are related by time-reversal symmetry.

We expand each molecular spinor in a primary basis of atomic orbitals (AO), $\{\chi_\mu\}_{\mu=1,\dots,N_{\text{bas}}}$, as

$$\phi_k(\mathbf{r}) = \begin{pmatrix} \phi_k^\uparrow(\mathbf{r}) \\ \phi_k^\downarrow(\mathbf{r}) \end{pmatrix} = \sum_\mu \begin{pmatrix} b_{k\uparrow\mu} \chi_\mu(\mathbf{r}) \\ b_{k\downarrow\mu} \chi_\mu(\mathbf{r}) \end{pmatrix} = \sum_\mu \begin{pmatrix} (b_{k\uparrow\mu}^R + i b_{k\uparrow\mu}^I) \chi_\mu(\mathbf{r}) \\ (b_{k\downarrow\mu}^R + i b_{k\downarrow\mu}^I) \chi_\mu(\mathbf{r}) \end{pmatrix}, \quad (18)$$

where \uparrow ($\sigma = \frac{1}{2}$) and \downarrow ($\sigma = -\frac{1}{2}$) denote the different projections of spin on the z -axis. Each spinor ϕ_k can be related by the time-reversal symmetry or Kramers' operator \hat{K} to a

Kramers' partner $\phi_{\bar{k}}$ with the same energy, $\epsilon_k = \epsilon_{\bar{k}}$,

$$\hat{K}\phi_k = \begin{pmatrix} \phi_k^\uparrow(\mathbf{r}) \\ \phi_k^\downarrow(\mathbf{r}) \end{pmatrix} = \begin{pmatrix} -\phi_k^{\downarrow*}(\mathbf{r}) \\ \phi_k^{\uparrow*}(\mathbf{r}) \end{pmatrix} = \begin{pmatrix} -\phi_k^{\downarrow,R}(\mathbf{r}) + i\phi_k^{\downarrow,I}(\mathbf{r}) \\ \phi_k^{\uparrow,R}(\mathbf{r}) - i\phi_k^{\uparrow,I}(\mathbf{r}) \end{pmatrix} = \phi_{\bar{k}}. \quad (19)$$

Using quaternion algebra it is possible to reduce the dimension of matrices that need to be considered to half the original size.¹⁰⁶ Alternatively, one may keep the full dimension, but use the spinor pairing to define matrices as either real or imaginary. We will take the latter approach in this work. Denoting pairs of spinors with (p, \bar{p}) , noting that $\hat{K}\phi_{\bar{p}} = -\phi_p$ and transforming a purely imaginary diagonal operator A that obeys $A_{pp} = A_{\bar{p}\bar{p}}$ and $A_{pp} = -A_{\bar{p}\bar{p}}^*$ we can deduce

$$\begin{aligned} A_{\mu\nu,\uparrow\uparrow} &= \sum_p b_{p\uparrow\mu} A_{pp} b_{p\uparrow\nu}^* + \sum_{\bar{p}} b_{\bar{p}\uparrow\mu} A_{\bar{p}\bar{p}} b_{\bar{p}\uparrow\nu}^* = \sum_{\bar{p}} b_{\bar{p}\downarrow\mu}^* A_{\bar{p}\bar{p}} b_{\bar{p}\downarrow\nu} + \sum_p b_{p\downarrow\mu}^* A_{pp} b_{p\downarrow\nu} = -A_{\mu\nu,\downarrow\downarrow}^* \\ A_{\mu\nu,\downarrow\uparrow} &= \sum_p b_{p\downarrow\mu} A_{pp} b_{p\uparrow\nu}^* + \sum_{\bar{p}} b_{\bar{p}\downarrow\mu} A_{\bar{p}\bar{p}} b_{\bar{p}\uparrow\nu}^* = -\sum_p b_{\bar{p}\uparrow\mu}^* A_{\bar{p}\bar{p}} b_{\bar{p}\downarrow\nu} - \sum_{\bar{p}} b_{p\uparrow\mu}^* A_{pp} b_{p\downarrow\nu} = A_{\mu\nu,\uparrow\downarrow}^*. \end{aligned} \quad (20)$$

It is convenient to split this operator into real and imaginary components, and we use the character of the MO coefficient products to label real (superscript R) and imaginary (superscript I) parts of the operator,

$$A_{\mu\nu,\sigma\sigma'}^R = \sum_p b_{p\sigma\mu}^R A_{pp} b_{p\sigma'\nu}^R + \sum_{\bar{p}} b_{\bar{p}\sigma\mu}^R A_{\bar{p}\bar{p}} b_{\bar{p}\sigma'\nu}^R + \sum_p b_{p\sigma\mu}^I A_{pp} b_{p\sigma'\nu}^I + \sum_{\bar{p}} b_{\bar{p}\sigma\mu}^I A_{\bar{p}\bar{p}} b_{\bar{p}\sigma'\nu}^I \quad (21)$$

and

$$A_{\mu\nu,\sigma\sigma'}^I = \sum_p b_{p\sigma\mu}^R A_{pp} b_{p\sigma'\nu}^I + \sum_{\bar{p}} b_{\bar{p}\sigma\mu}^R A_{\bar{p}\bar{p}} b_{\bar{p}\sigma'\nu}^I - \sum_p b_{p\sigma\mu}^I A_{pp} b_{p\sigma'\nu}^R - \sum_{\bar{p}} b_{\bar{p}\sigma\mu}^I A_{\bar{p}\bar{p}} b_{\bar{p}\sigma'\nu}^R. \quad (22)$$

The time-ordered single-particle Green's function fulfills eq. (20) and therefore in AO basis

obeys the relations

$$\begin{aligned}
G_{\mu\nu,\uparrow\uparrow}^{\leq}(i\tau) &= -G_{\mu\nu,\downarrow\downarrow}^{\leq*}(i\tau) \\
G_{\mu\nu,\uparrow\downarrow}^{\leq}(i\tau) &= G_{\mu\nu,\downarrow\uparrow}^{\leq*}(i\tau).
\end{aligned}
\tag{23}$$

Convenient is sometimes also to re-express these quantities in a spin matrix basis. We then get (denoting the unit matrix as 0, and the Pauli spin matrices as x, y and z)

$$\begin{aligned}
G_{\mu\nu}^{\leq 0}(i\tau) &= G_{\mu\nu,\uparrow\uparrow}^{\leq}(i\tau) + G_{\mu\nu,\downarrow\downarrow}^{\leq}(i\tau) = 2G_{\mu\nu,\uparrow\uparrow}^{\leq R}(i\tau), \\
G_{\mu\nu}^{\leq x}(i\tau) &= G_{\mu\nu,\uparrow\downarrow}^{\leq}(i\tau) + G_{\mu\nu,\downarrow\uparrow}^{\leq}(i\tau) = 2G_{\mu\nu,\uparrow\downarrow}^{\leq I}(i\tau), \\
G_{\mu\nu}^{\leq y}(i\tau) &= iG_{\mu\nu,\uparrow\downarrow}^{\leq}(i\tau) - iG_{\mu\nu,\downarrow\uparrow}^{\leq}(i\tau) = 2iG_{\mu\nu,\uparrow\downarrow}^{\leq R}(i\tau), \\
G_{\mu\nu}^{\leq z}(i\tau) &= G_{\mu\nu,\uparrow\uparrow}^{\leq}(i\tau) - G_{\mu\nu,\downarrow\downarrow}^{\leq}(i\tau) = 2G_{\mu\nu,\uparrow\uparrow}^{\leq I}(i\tau),
\end{aligned}
\tag{24}$$

which more clearly shows the relation to 1-component theories in which only the first Green's function has a non-zero value.

Polarizability in imaginary time

We next consider the polarizability.^{71,72,107} Whereas in the complete formalism of Aryasetiawan and Biermann⁷¹ the polarizability includes the response of the charge density to magnetic fields as well as the induction of current densities, both of these are considered strictly zero in a Kramers-restricted formalism. We can then define the relevant part of the polarizability in AO basis as

$$P_{\mu\nu\sigma,\kappa\lambda\sigma'}^{(0)}(i\tau) = i\Theta(\tau)G_{\mu\kappa,\sigma\sigma'}^>(i\tau)G_{\nu\lambda,\sigma'\sigma}^<(-i\tau) + i\Theta(-\tau)G_{\mu\kappa,\sigma\sigma'}^<(i\tau)G_{\nu\lambda,\sigma'\sigma}^>(-i\tau). \tag{25}$$

Due to the symmetry $P^{(0)}(i\tau) = P^{(0)}(-i\tau)$, we can focus on the first term which we split in terms of real (R) and imaginary (I) components

$$\begin{aligned}
G_{\mu\kappa,\sigma\sigma'}^>(i\tau)G_{\nu\lambda,\sigma'\sigma}^<(-i\tau) &= G_{\mu\kappa,\sigma\sigma'}^>^R(i\tau)G_{\nu\lambda,\sigma'\sigma}^<^R(-i\tau) - G_{\mu\kappa,\sigma\sigma'}^>^I(i\tau)G_{\nu\lambda,\sigma'\sigma}^<^I(-i\tau) \\
&+ iG_{\mu\kappa,\sigma\sigma'}^>^I(i\tau)G_{\nu\lambda,\sigma'\sigma}^<^R(-i\tau) + iG_{\mu\kappa,\sigma\sigma'}^>^R(i\tau)G_{\nu\lambda,\sigma'\sigma}^<^I(-i\tau).
\end{aligned}
\tag{26}$$

Kramers symmetry implies

$$\sum_{\sigma, \sigma' = \uparrow, \downarrow} iG_{\mu\sigma, \kappa\sigma'}^{>I}(i\tau)G_{\nu\sigma', \lambda\sigma}^{<R}(-i\tau) + iG_{\mu\sigma, \kappa\sigma'}^{>R}(i\tau)G_{\nu\sigma', \lambda\sigma}^{<I}(-i\tau) = 0, \quad (27)$$

as well as

$$\begin{aligned} P_{\mu\nu\uparrow, \kappa\lambda\uparrow}^{(0)}(i\tau) &= P_{\mu\nu\downarrow, \kappa\lambda\downarrow}^{(0)}(i\tau) \\ P_{\mu\nu\uparrow, \kappa\lambda\downarrow}^{(0)}(i\tau) &= P_{\mu\nu\downarrow, \kappa\lambda\uparrow}^{(0)}(i\tau). \end{aligned} \quad (28)$$

We proof these relations in appendix A. Already in the primary AO basis this would reduce the number of matrix elements that are to be calculated considerably. Further efficiency can be gained by expanding the polarizability and the Coulomb potential in a basis of auxiliary functions $\{f_\alpha\}_{\alpha=1, \dots, N_{\text{aux}}}$ with products of primary basis functions being expressed as

$$\chi_\mu(\mathbf{r})\chi_\nu(\mathbf{r}) = \sum_\alpha c_{\mu\nu\alpha} f_\alpha(\mathbf{r}). \quad (29)$$

To calculate the fitting coefficients, we use the pair-atomic density fitting (PADF) method^{108–113} in the implementation of ref. 114. The following working equations are however completely general and can be implemented using any type of density fitting (DF). For instance, global density fitting using the overlap kernel¹¹⁵ (also known as RI-SVS) or the attenuated Coulomb kernel^{116,117} which have already been used to achieve low-scaling *GW* implementations^{18,19} would be suitable choice as well.

For the polarizability we can eliminate the explicit dependence on spin in the transformation to the auxiliary basis and work with the spin-summed form

$$P_{\alpha\beta}^{(0)}(i\tau) = \sum_{\sigma\sigma' = \uparrow, \downarrow} c_{\mu\nu\alpha} P_{\mu\kappa\sigma, \nu\lambda\sigma'}^{(0)}(i\tau) c_{\kappa\lambda\beta}. \quad (30)$$

Likewise we define spin-independent representations of the Coulomb potential and screened

interaction in the auxiliary basis as

$$v_{\alpha\beta} = \int d\mathbf{r}d\mathbf{r}' f_{\alpha}(\mathbf{r})v_c(\mathbf{r}, \mathbf{r}')f_{\beta}(\mathbf{r}') \quad (31)$$

$$W_{\alpha\beta}(i\tau) = \int d\mathbf{r}d\mathbf{r}' f_{\alpha}(\mathbf{r})W(\mathbf{r}, \mathbf{r}', i\tau)f_{\beta}(\mathbf{r}') , \quad (32)$$

Our final expression for the polarizability is

$$P_{\alpha\beta}^{(0)}(i\tau) = -2ic_{\mu\nu\alpha} \left\{ G_{\mu\kappa,\uparrow\uparrow}^{>R}(i\tau)G_{\nu\lambda,\uparrow\uparrow}^{<R}(i\tau) - G_{\mu\kappa,\uparrow\uparrow}^{>I}(i\tau)G_{\nu\lambda,\uparrow\uparrow}^{<I}(i\tau) \right. \\ \left. + G_{\mu\kappa,\uparrow\downarrow}^{>R}(i\tau)G_{\nu\lambda,\uparrow\downarrow}^{<R}(i\tau) - G_{\mu\kappa,\uparrow\downarrow}^{>I}(i\tau)G_{\nu\lambda,\uparrow\downarrow}^{<I}(i\tau) \right\} c_{\kappa\lambda\beta} , \quad (33)$$

or equivalently

$$P_{\alpha\beta}^{(0)}(i\tau) = -\frac{1}{2}ic_{\mu\nu\alpha} \left\{ G_{\mu\kappa}^{>0}(i\tau)G_{\nu\lambda}^{<0}(i\tau) - G_{\mu\kappa}^{>x}(i\tau)G_{\nu\lambda}^{<x}(i\tau) \right. \\ \left. - G_{\mu\kappa}^{>y}(i\tau)G_{\nu\lambda}^{<y}(i\tau) - G_{\mu\kappa}^{>z}(i\tau)G_{\nu\lambda}^{<z}(i\tau) \right\} c_{\kappa\lambda\beta} . \quad (34)$$

The first term in this expression is equivalent in the spin-restricted 1C formalism.¹⁵ Evaluation of (33) or (34) is therefore exactly four times more expensive than in a scalar relativistic calculation. Equation (33) can be implemented with quadratic scaling with system size using PADF.¹⁵

Polarizability in imaginary frequency and MO basis

The AO based implementation of the polarizability is advantageous for rather large molecules only and it is computationally not efficient for the molecules in the SOC81 database typically containing just a few often heavy atoms. The AO based algorithms become advantageous when the local nature of the atomic orbitals can be exploited.¹⁵ This is only possible when the system is spatially extended and many functions in the basis set decay fast with the distance from the nucleus on which they are centered.

Especially for small systems with many heavy atoms, implementations in the canonical

basis are much faster since in those systems the locality of the AO basis cannot be exploited. For this reason we also implemented the polarizability in the MO representation. In the following, we will use $i, j \dots$ to label occupied, and $a, b \dots$ to label virtual orbitals. Using eq. (12) and these indices, eq. (25) becomes

$$P_{aiai}^{(0)}(i\tau) = -i\Theta(\tau)e^{-(\epsilon_a - \epsilon_i)\tau} - i\Theta(-\tau)e^{-(\epsilon_i - \epsilon_a)\tau} \quad (35)$$

in the MO basis. Using (9), the corresponding expression on the imaginary frequency axis is

$$P_{aiai}^{(0)}(i\omega) = -\frac{1}{\epsilon_a - \epsilon_i - i\omega} - \frac{1}{\epsilon_a - \epsilon_i + i\omega} . \quad (36)$$

Using the last equation on the *r.h.s.* of (18) and (29), we can write down a transformation from the auxiliary basis to the MO basis as

$$\phi_i^\dagger(\mathbf{r})\phi_a(\mathbf{r}) = \sum_{\alpha} c_{ia\alpha} f_{\alpha}(\mathbf{r}) \quad (37)$$

with

$$\begin{aligned} c_{ia\alpha} &= \sum_{\mu\kappa} (b_{i\uparrow\mu}^* b_{a\uparrow\kappa} + b_{i\downarrow\mu}^* b_{a\downarrow\kappa}) c_{\mu\kappa\alpha} = c_{ia\alpha}^R + i c_{ia\alpha}^I \\ &= \sum_{\mu\kappa} (b_{i\uparrow\mu}^R b_{a\uparrow\kappa}^R + b_{i\uparrow\mu}^I b_{a\uparrow\kappa}^I + b_{i\downarrow\mu}^R b_{a\downarrow\kappa}^R + b_{i\downarrow\mu}^I b_{a\downarrow\kappa}^I) c_{\mu\kappa\alpha} \\ &\quad + i \sum_{\mu\kappa} (b_{i\uparrow\mu}^R b_{a\uparrow\kappa}^I - b_{i\uparrow\mu}^I b_{a\uparrow\kappa}^R + b_{i\downarrow\mu}^R b_{a\downarrow\kappa}^I - b_{i\downarrow\mu}^I b_{a\downarrow\kappa}^R) c_{\mu\kappa\alpha} . \end{aligned} \quad (38)$$

Using this expression, eq. (36) becomes

$$\begin{aligned} P_{\alpha\beta}^{(0)}(i\omega) &= c_{ai\alpha} P_{aiai}^{(0)}(i\omega) c_{ai\beta} \\ &= 2 \left\{ c_{ia\alpha}^R \text{Re} P_{aiai}^{(0)} - c_{ia\alpha}^I \text{Im} P_{aiai}^{(0)} \right\} c_{ia\beta}^R + 2 \left\{ c_{ia\alpha}^R \text{Im} P_{aiai}^{(0)} + c_{ia\alpha}^I \text{Re} P_{aiai}^{(0)} \right\} c_{ia\beta}^I . \end{aligned} \quad (39)$$

Screened interaction and self-energy

If necessary, the polarizability is transformed to the imaginary frequency axis where the screened interaction is calculated in the basis of auxiliary functions using eq. (5),

$$W_{\alpha\beta}(i\omega) = v_{\alpha\beta} + \sum_{\gamma\delta} v_{\alpha\gamma} P_{\gamma\delta}^{(0)}(i\omega) W_{\delta\gamma}(i\omega) . \quad (40)$$

For the evaluation of the self-energy, we partition the screened Coulomb interaction as

$$\widetilde{W} = W - v . \quad (41)$$

This allows us to use different approximations for the dynamical and static contributions to the self-energy. To evaluate the self-energy on the imaginary frequency axis, we first define the time-ordered self-energy¹¹⁸

$$\Sigma_{xc}(i\tau) = \Sigma_x + \Theta(\tau)\Sigma_c^>(i\tau) - \Theta(-\tau)\Sigma_c^<(i\tau) . \quad (42)$$

Here, the greater and lesser components of the self-energy are given by

$$[\Sigma_c^{\lessgtr}]_{\mu\nu,\sigma\sigma'}(i\tau) = iG_{\kappa\lambda,\sigma\sigma'}^{\lessgtr}(i\tau)c_{\mu\kappa\alpha}\widetilde{W}_{\alpha\beta}(i\tau)c_{\nu\lambda\beta} , \quad (43)$$

and the singular contribution (Fock term) as

$$[\Sigma_x]_{\mu\nu,\sigma\sigma'} = iG_{\kappa\lambda,\sigma\sigma'}^<(i\tau \rightarrow 0^-)c_{\mu\kappa\alpha}v_{\alpha\beta}c_{\nu\lambda\beta} . \quad (44)$$

Dynamical contribution In the basis of Pauli matrices, (43) can be expanded as

$$[\Sigma_c^{\lessgtr}]_{\mu\nu}(i\tau) = i \begin{pmatrix} G_{\kappa\lambda}^{\lessgtr 0}(i\tau) + G_{\kappa\lambda}^{\lessgtr z}(i\tau) & G_{\kappa\lambda}^{\lessgtr x}(i\tau) - iG_{\kappa\lambda}^{\lessgtr y}(i\tau) \\ G_{\kappa\lambda}^{\lessgtr x}(i\tau) + iG_{\kappa\lambda}^{\lessgtr y}(i\tau) & G_{\kappa\lambda}^{\lessgtr 0}(i\tau) - G_{\kappa\lambda}^{\lessgtr z}(i\tau) \end{pmatrix} c_{\mu\kappa\alpha}\widetilde{W}_{\alpha\beta}(i\tau)c_{\nu\lambda\beta} . \quad (45)$$

In the correlation part of the self-energy we only calculate the contribution due to $G^{\leq 0}$, i.e., $G^{\leq x}, G^{\leq y}, G^{\leq z}$ are set to zero. Therefore, using (24), eq. (45) reduces to

$$[\Sigma_c^{\leq}]_{\mu\nu}(i\tau) = 2i \begin{pmatrix} G_{\kappa\lambda,\uparrow\uparrow}^{\leq R}(i\tau) & 0 \\ 0 & G_{\kappa\lambda,\uparrow\uparrow}^{\leq R}(i\tau) \end{pmatrix} c_{\mu\kappa\alpha} \widetilde{W}_{\alpha\beta}(i\tau) c_{\nu\lambda\beta}. \quad (46)$$

This quantity has the form as in the 1C formalism and in the same way as in our 1C implementation.¹⁵ Notice also, that $G^{\leq R}$ has a prefactor of $-i$ due to the definitions eqs. (13) and (14). We Fourier transform (43) to the imaginary frequency axis using eq. (9), for which we follow the treatment of Liu et al.¹¹⁹ From there, the self-energy is transformed back to the MO basis and analytically continued to real frequencies using the algorithm by Vidberg and Serene.¹²⁰ For details on the AC for G_0W_0 and qsGW we refer to our previous work.^{15,16}

Hartree-exchange contribution Equation (44) is recovered from (45) by replacing $\widetilde{W}(i\tau)$ with v_c and using $D = G^<(i\tau \rightarrow 0^-)$ instead of $G^<(i\tau)$. The resulting expression is identical to the ones typically implemented in 2C-Hartree-Fock codes,^{121,122}

$$[\Sigma_x]_{\mu\nu} = \begin{pmatrix} D_{\kappa\lambda}^0 + D_{\kappa\lambda}^z & D_{\kappa\lambda}^x - iD_{\kappa\lambda}^y \\ D_{\kappa\lambda}^x + iD_{\kappa\lambda}^y & D_{\kappa\lambda}^0 - D_{\kappa\lambda}^z \end{pmatrix} c_{\mu\kappa\alpha} v_{\alpha\beta} c_{\nu\lambda\beta} \quad (47)$$

where the different components of D are obtained as the $i\tau \rightarrow 0$ limit of eq. (24). In qsGW, we also need to evaluate the block-diagonal Hartree-contribution to the self-energy,

$$[\Sigma_H]_{\mu\nu} = \begin{pmatrix} D_{\kappa\lambda}^0 & \\ & D_{\kappa\lambda}^0 \end{pmatrix} c_{\mu\nu\alpha} v_{\alpha\beta} c_{\kappa\lambda\beta} \quad (48)$$

The full qsGW Hamiltonian is then constructed according to eq. (17) and eq. (72) is solved in the MO basis from the previous iteration. The new set of MO expansion coefficients and QP energies is then used to evaluate eq. (24) in the next iteration.

The $G3W2$ Correction

As explained in ref. 49, we evaluate the contribution of the $G3W2$ term to the self-energy as a perturbative correction to the solution of the GWA. Relying on the assumption that GW already gives rather accurate QP energies we expand Σ^{G3W2} around the GW QP energies and obtain

$$\epsilon_p^{GW+G3W2} = \epsilon_p^{GW} + \Sigma_{pp}^{G3W2}(\epsilon_p^{GW}), \quad (49)$$

at zeroth order where Σ_{pp}^{G3W2} is evaluated using the GW QP energies obtained from the solution of (15) or (16). We restrict ourselves to the statically screened $G3W2$ self-energy which is obtained from (4) by replacing both $W(1,2)$ with $W(1,2)\delta(t_1 - t_2)$.⁴⁹ In terms of $G^{(s)}$ and in a basis of single-particle states (In case of G_0W_0 or $evGW$ this would be the basis of KS states, in case of $qsGW$ the basis of $qsGW$ eigenstates), this term becomes¹²³

$$\Sigma_{pp}^{G3W2}(\epsilon_p) = \sum_i^{occ} \sum_{ab}^{virt} \frac{W(i\omega = 0)_{paib} W(i\omega = 0)_{aibp}}{\epsilon_a + \epsilon_b - \epsilon_i - \epsilon_p} - \sum_{ij}^{occ} \sum_a^{virt} \frac{W(i\omega = 0)_{piaj} W(i\omega = 0)_{iajp}}{\epsilon_a - \epsilon_i - \epsilon_j + \epsilon_p}, \quad (50)$$

with

$$W(i\omega = 0)_{pqrs} = \int d\mathbf{r} d\mathbf{r}' \phi_p(\mathbf{r}) \phi_q^\dagger(\mathbf{r}) W(\mathbf{r}, \mathbf{r}', i\omega = 0) \phi_r(\mathbf{r}') \phi_s^\dagger(\mathbf{r}'). \quad (51)$$

Using the transformation eqs. (37) and (38) we write (51) as

$$W(i\omega = 0)_{pqrs} = \sum_{\alpha} d_{pq\alpha} c_{rs\beta}, \quad (52)$$

with

$$d_{pq\alpha} = \sum_{\beta} c_{pq\beta} W(i\omega = 0)_{\alpha\beta}. \quad (53)$$

When complex matrix algebra is used, inserting this transformation into (50) increases the computational effort by a factor of 16 (notice that the denominator is always real) compared to the 1C case. To reduce the computational effort, we use real matrix algebra and define

the intermediates

$$\begin{aligned}
W_{pqrs}^{R/I,R/I} &= \sum_{\alpha} d_{pq\alpha}^{R/I} c_{rs\beta}^{R/I} \\
e_{pqrs} &= W_{pqrs}^{R,R} - W_{pqrs}^{I,I} \\
f_{pqrs} &= W_{pqrs}^{R,I} + W_{pqrs}^{I,R} .
\end{aligned} \tag{54}$$

The final self-energy correction (50) is then evaluated as

$$\Sigma_{pp}^{G3W2}(\epsilon_p) = \sum_i \sum_{ab}^{occ\ virt} \frac{e_{paib} e_{aibp} - f_{paib} f_{aibp}}{\epsilon_a + \epsilon_b - \epsilon_i - \epsilon_p} - \sum_{ij} \sum_a^{occ\ virt} \frac{e_{piaj} e_{iajp} - f_{piaj} f_{iajp}}{\epsilon_a - \epsilon_i - \epsilon_j + \epsilon_p} . \tag{55}$$

Here, the by far most expensive step is the calculation of the first four intermediates defined in the first equation of (54). Therefore, evaluating (55) is four times more expensive than the corresponding 1C expression.

3 Computational Details

Choice of 2C-Hamiltonian

The 2C *GW* equations have been implemented in a locally modified development version of the Slater Type orbital (STO) based ADF engine¹²⁴ within the Amsterdam modeling suite (AMS2022).¹²⁵ In principle, the implementation is independent of the choice of the particular choice of the 2C Hamiltonian. In the work, we use the zeroth-order regular approximation (ZORA) Hamiltonian by van Lenthe et al,^{126–128} which can be written as¹²⁸

$$\hat{h}_1^{ZORA}(\mathbf{r}) = \hat{h}_1^{ZORA,SR}(\mathbf{r}) + \hat{h}_1^{ZORA,SO}(\mathbf{r}) . \tag{56}$$

The first term,

$$\hat{h}_1^{ZORA,SR}(\mathbf{r}) = v_{ext}(\mathbf{r}) + \vec{p} \frac{c^2}{2c^2 - v_{ext}(\mathbf{r})} \vec{p} \tag{57}$$

describes scalar relativistic effects and we use this Hamiltonian in all 1C calculations. The second term

$$\hat{h}_1^{ZORA,SO}(\mathbf{r}) = \frac{c^2}{(2c^2 - v_{ext}(\mathbf{r}))^2} \vec{\sigma} \cdot (\nabla v_{ext}(\mathbf{r}) \times \vec{p}) \quad (58)$$

accounts for SOC. We employ the Hamiltonian (56) in all of the following 2C calculations. We also tested two Hamiltonians obtained from an exact transformation of the 4-component Dirac equation to 2-components (X2C and RA-X2C, respectively. In the latter variant, a regular approach to calculate the transformation matrix is used).^{129,130} In the X2C and RA-X2C method implemented in ADF, first the 4-component Dirac equation for a model potential (MAPA) of the molecule is calculated for the given basis set, using the modified Dirac equation (MDE) by Dyll¹³¹ for X2C, or using the regular approach¹³² to the modified Dirac equation (RA-MDE) for RA-X2C. In the basis set limit the MDE and the RA-MDE should yield same results for the model potential (MAPA) but using a finite basis set, the results for MDE and RA-MDE will differ.¹³³ In a next step, these 4-component equations are transformed to a 2C form.¹³⁴ We found, that the particular choice of 2C Hamiltonian (ZORA, X2C or RA-X2C) only affects the final ionization potentials (IP) by a few 10 meV.

Basis Sets

In all calculations, we expand the spinors in (18) in all-electron STO basis sets of triple- and quadruple- ζ quality (TZ3P and QZ6P, respectively).¹³⁵ The STO type basis sets in ADF are restricted to a maximum angular momentum of $l = 3$, which complicates reaching the basis set limit for individual QP energies.^{41,136} This is especially true for heavier elements with occupied d - or f -shells where higher angular momenta functions are needed to polarize the basis.¹³⁷

The numerical atomic orbital (NAO) based BAND engine^{138,139} of AMS can be used with basis functions of arbitrary angular momenta. To obtain converged QP energies we therefore augment our TZ3P and QZ6P basis sets with higher angular momenta functions

and calculate scalar relativistic QP energies. In the choice of the higher angular momenta functions we follow the construction of the Sapporo-DKH3-(T,Q)ZP-2012 basis sets^{140,141} for all elements in the fourth to the sixth row of the periodic table. In the following we denote these basis sets as TZ3P+ and QZ6P+. Except for the Lanthanides, where the highest angular momenta are $l = 5$ and $l = 6$, the augmented TZ (QZ) basis set typically contains basis functions with angular momentum up to $l = 4$ ($l = 5$) for elements beyond the third row. The basis set definitions are included in the supporting information.

To calculate our final QP energies we first calculate complete basis set (CBS) limit extrapolated scalar relativistic QP energies with the BAND code using the expression

$$\epsilon_n^{GW,scalar}(CBS) = \epsilon_n^{GW,scalar}(QZ6P+) - \frac{\epsilon_n^{GW,scalar}(QZ6P+) - \epsilon_n^{GW,scalar}(TZ3P+)}{1 - \frac{N_{bas}^{QZ}}{N_{bas}^{TZ}}}, \quad (59)$$

where $\epsilon_n^{GW,scalar}(QZ6P+)$ ($\epsilon_n^{GW,scalar}(TZ3P+)$) denotes the value of the QP energy calculated with QZ6P+ (TZ3P+) and N_{bas}^{QZ} and N_{bas}^{TZ} denote the respective numbers of basis functions (in spherical harmonics so that there are e.g. 5 d and 7 f functions). This expression is commonly used for the extrapolation of GW QP energies to the complete basis set limit for localized basis functions.³⁷ Spin-orbit corrections Δ_n^{2C} are then calculated with ADF using the QZ6P basis set,

$$\Delta_n^{2C}(QZ6P) = \epsilon_n^{GW,scalar}(QZ6P) - \epsilon_n^{GW,2C}(QZ6P) \quad (60)$$

The corresponding QP energies are then obtained as

$$\epsilon_n^{GW,2C}(CBS) = \epsilon_n^{GW,scalar}(CBS) + \Delta_n^{2C}(QZ6P) \quad (61)$$

$$\epsilon_n^{GW+G3W2,2C}(CBS) = \epsilon_n^{GW,2C}(CBS) + \Sigma_{nn}^{G3W2}(QZ6P). \quad (62)$$

This choice is well justified since the major part correction to the KS QP energies comes from the scalar relativistic part of the GW correction. The spin-orbit correction and the

G_3W_2 corrections are typically of the order of only a few hundred meV in magnitude (also see explicit values in the supporting information). Therefore, even relatively large errors in these quantities while only have a minor effect on the final results.

Technical Details

We perform G_0W_0 calculations using PBE, PBE0 and BHLYP¹⁴² orbitals and eigenvalues. The latter functional contains 50 % of exact exchange which is typically the optimal fraction for G_0W_0 QP energies for organic molecules.^{44,82,143} $evGW$ and $qsGW$ calculations are performed starting from PBE0 orbitals and eigenvalues. In all calculations we set the numerical quality to *VeryGood*.¹²³ The auxiliary bases used to expand 4-point correlation functions are automatically generated from products of primary basis functions. For this, we use a variant of an algorithm introduced in ref. 113 which has recently been implemented in ADF and BAND.¹¹⁴ The size of the auxiliary basis in this approach can be tuned by a single threshold which we set to $\epsilon_{aux} = 1 \times 10^{-10}$ in all partially self-consistent calculations and to $\epsilon_{aux} = 1 \times 10^{-8}$ for G_0W_0 . This corresponds to a very large auxiliary basis which is typically around 12 times larger than the primary basis and eliminates PADF errors for relative energies of medium molecules almost completely.¹¹⁴

Imaginary time and imaginary frequency variables are discretized using non-uniform bases $\mathcal{T} = \{\tau_\alpha\}_{\alpha=1,\dots,N_\tau}$ and $\mathcal{W} = \{\omega_\alpha\}_{\alpha=1,\dots,N_\omega}$ of sizes N_τ and N_ω , respectively, tailored to each system. More precisely, (9) is implemented as

$$\overline{F}(i\omega_\alpha) = \Omega_{\alpha\beta}^{(c)} \overline{F}(i\tau_\beta) \quad (63)$$

$$\underline{F}(i\omega_\alpha) = \Omega_{\alpha\beta}^{(s)} \underline{F}(i\tau_\beta), \quad (64)$$

where \overline{F} and \underline{F} denote even and odd parts of F . The transformation from imaginary frequency to imaginary time only requires the (pseudo)inversion of $\Omega^{(c)}$ and $\Omega^{(s)}$, respectively. Our procedure to calculate $\Omega^{(c)}$ and $\Omega^{(s)}$ as well as \mathcal{T} and \mathcal{W} follows Kresse and coworkers

ers.^{119,144,145} The technical specifications of our implementation have been described in the appendix of ref. 135.

Convergence acceleration

For the molecules in the SOC81 set, we have found that the *evGW* and *evGW*₀ calculations converge within 5-8 iterations within an accuracy of a few meV when the DIIS implementation of ref. 146 is used. All *evGW* results presented in this work have been obtained using this DIIS implementation with a convergence criterion of 3 meV.

On the other hand, using our own DIIS implementation of ref. 16 the *qsGW* equations often do not converge for the systems in the SOC81 set. As discussed in the literature,^{135,147} this issue is related to multiple QP solutions which seem to occur frequently in systems containing heavy elements. More sophisticated DIIS algorithms might offer a solution to this problem.¹⁴⁸ In addition to the switching between the QP peaks there is additional numerical strain which most likely arises from precision issues from the AC of the self-energy. Especially problematic are the off-diagonal elements of the self-energy matrix which should be zero at convergence. For a more detailed discussion we refer to our previous work.¹⁶

In this work, we have found a linear mixing strategy with adaptive mixing parameter α_{mix} to lead to stable convergence of the *qsGW* SCF procedure after typically around 15 iterations. Specifically, we start the self-consistency cycle with $\alpha_{mix}^{(0)} = 0.3$. In case the SCF error decreases, we use the mixing parameter $\alpha_{mix}^{(n)} = \max \left\{ 1.2 \times \alpha_{mix}^{(n-1)}, 0.5 \right\}$ in the *n*th iteration. In case the SCF error increases, we reset the mixing parameter to $\alpha_{mix}^{(0)}$.

4 Results

Comparison to WEST

In this section 4, we compare our results for SOC81 to the ones calculated by Scherpelz et al.⁷⁴ with the WEST code.^{21,24}

Multi-solution Cases

Before discussing the results in detail, we notice that Scherpelz and Govoni identified in total 14 systems¹⁴⁹ in the SOC81 set for which the non-linear QP equations (15) have multiple solutions for $G_0W_0@PBE$.⁷⁴ All of these solutions can be found graphically in the sum-over-states formalism (analytical integration of the self-energy)^{8,150,151} or contour deformation techniques,^{21,50,74,152} by plotting the self-energy matrix elements as a function of frequency. Also in cases where QP spectra are calculated with different basis sets it is possible to identify the matching peaks in individual spectra and perform a reliable extrapolation to the CBS limit.

AC, however, typically fails to detect all solutions in these cases. Furthermore, the resulting QP energies will be rather inaccurate since it is impossible to build a Padé model which reliably represents the energy dependence of self-energy matrix elements with strongly varying frequency dependence (see ref. 74 for examples).^{50,153}

The occurrence of multiple solutions can be an artefact of the starting point used in a G_0W_0 calculation.³⁹ It can also be caused by a break-down of the single QP picture caused by pronounced static correlation effects. The occurrence of multiple solutions complicates the comparison of our results to WEST, since it is not clear if the same solutions are compared. It also complicates the extrapolation of results to the CBS limit since it is unclear if the same QP solution is found for all basis sets. Also comparison to experimental data is difficult since it is unclear if the detected solutions correspond to QP or to satellite peaks in the experimental spectra. For all these reasons, we decided to exclude these systems from the following benchmark. This leaves us with 67 systems to which we refer to as SOC81*.

Scalar relativistic Ionization potentials

Table 1: Scalar relativistic and 2C G_0W_0 @PBE and G_0W_0 @PBE0 ionization potentials (IP) for the SOC81* database calculated with ADF/BAND. The corresponding values from WEST are given for comparison. All values are in eV.

Name	ADF/BAND				WEST			
	scalar		2C		scalar		2C	
	G_0W_0 @ PBE	G_0W_0 @ PBE0	G_0W_0 @ PBE	G_0W_0 @ PBE0	G_0W_0 @ PBE	G_0W_0 @ PBE0	G_0W_0 @ PBE	G_0W_0 @ PBE0
Al ₂ Br ₆	10.32	10.73	10.30	10.70	10.38	10.78	10.34	10.74
AlBr ₃	10.47	10.85	10.44	10.81	10.53	10.91	10.48	10.86
AlI ₃	9.32	9.67	9.19	9.53	9.44	9.78	9.23	9.57
AsBr ₃	9.79	10.14	9.76	10.09	9.83	10.17	9.77	10.10
AsCl ₃	10.53	10.89	10.53	10.88	10.67	11.00	10.66	10.99
AsF ₃	12.38	12.80	12.38	12.80	12.49	12.89	12.49	12.89
AsF ₅	14.48	15.31	14.47	15.30	14.51	15.28	14.49	15.26
AsH ₃	10.42	10.54	10.42	10.54	10.33	10.55	10.33	10.54
AsI ₃	8.86	9.33	8.70	9.09	8.99	9.39	8.72	9.11
Br ₂	10.29	10.55	10.16	10.40	10.33	10.59	10.16	10.42
BrCl	10.69	10.98	10.59	10.87	10.79	11.06	10.67	10.93
C ₁₀ H ₁₀ Ru	6.89	8.72	6.89	8.72	7.00	–	6.90	–
C ₂ H ₂ Se	8.48	8.72	8.47	8.72	8.48	8.72	8.48	8.72
C ₂ H ₆ Cd	8.86	9.16	8.86	9.16	8.82	9.09	8.83	9.10
C ₂ H ₆ Hg	9.10	9.30	9.12	9.33	8.99	9.20	9.07	9.28
C ₂ H ₆ Se	8.14	8.38	8.14	8.38	8.17	8.41	8.12	8.41
C ₂ H ₆ Zn	9.42	9.70	9.42	9.70	9.38	9.65	9.38	9.65
C ₂ HBrO	9.04	9.36	9.03	9.35	8.98	9.28	8.97	9.27
C ₄ H ₄ Se	8.72	8.98	8.72	8.98	8.60	8.86	8.60	8.86
CF ₃ I	10.37	10.66	10.12	10.39	10.52	10.81	10.20	10.48
CH ₃ HgBr	9.56	9.98	9.48	9.87	9.72	10.11	9.59	9.97
CH ₃ HgCl	10.09	10.64	10.07	10.61	10.30	10.76	10.26	10.72
CH ₃ HgI	8.85	9.23	8.66	9.00	9.08	9.38	8.79	9.09
CH ₃ I	9.42	9.63	9.19	9.36	9.57	9.78	9.26	9.46
Cl ₄	8.86	9.26	8.64	9.05	8.91	9.28	8.76	9.04
CaBr ₂	9.66	10.10	9.58	9.99	9.80	10.24	9.67	10.10
CaI ₂	8.99	9.29	8.79	9.06	9.09	9.48	8.79	9.18
CdBr ₂	10.05	10.49	9.95	10.36	10.21	10.62	10.06	10.46
CdCl ₂	10.72	11.23	10.70	11.19	10.91	11.39	10.87	11.34
CdI ₂	9.29	9.62	9.06	9.36	9.41	9.76	9.09	9.43
CsF	8.49	9.51	8.49	9.50	8.24	9.08	8.24	9.08
HgCl ₂	10.66	11.08	10.61	11.02	10.93	11.35	10.85	11.28
I ₂	9.34	9.64	9.05	9.34	9.41	9.64	9.01	9.26
IBr	9.70	9.95	9.45	9.69	9.81	10.04	9.51	9.73
ICl	9.99	10.24	9.74	9.97	10.14	10.37	9.85	10.07
IF	10.44	10.66	10.14	10.34	10.55	10.80	10.23	10.47
Kr ₂	13.28	13.57	13.19	13.45	13.42	13.68	13.27	13.53
KrF ₂	12.56	13.28	12.50	13.22	12.58	13.30	12.51	13.22
LaBr ₃	9.80	10.32	9.77	10.24	9.90	10.41	9.82	10.31
LaCl ₃	10.58	11.17	10.57	11.15	10.73	11.26	10.72	11.24
LiBr	8.79	9.16	8.70	9.05	8.95	9.35	8.81	9.21
LiI	8.10	8.48	7.90	8.25	8.35	8.65	8.04	8.36
MgBr ₂	10.37	10.79	10.27	10.67	10.49	10.91	10.35	10.76
MgI ₂	9.52	9.87	9.30	9.62	9.62	9.97	9.31	9.65
MoC ₆ O ₆	8.55	12.44	8.52	9.86	8.55	–	8.50	–
OsO ₄	11.82	12.44	11.82	12.42	11.74	12.41	11.74	12.41

Continued on next page

Name	ADF/BAND				WEST			
	scalar		2C		scalar		2C	
	$G_0W_0@$ PBE	$G_0W_0@$ PBE0	$G_0W_0@$ PBE	$G_0W_0@$ PBE0	$G_0W_0@$ PBE	$G_0W_0@$ PBE0	$G_0W_0@$ PBE	$G_0W_0@$ PBE0
PBr ₃	9.56	9.89	9.54	9.86	9.60	9.92	9.57	9.88
POBr ₃	10.57	11.05	10.51	10.93	10.55	11.01	10.49	10.93
RuO ₄	11.48	12.24	11.48	12.24	11.45	12.19	11.44	12.18
SOBr ₂	10.12	10.58	9.97	10.52	10.17	10.57	10.13	10.52
SPBr ₃	9.47	9.77	9.45	9.75	9.45	9.82	9.43	9.79
SeCl ₂	9.13	9.45	9.10	9.43	9.24	9.53	9.24	9.53
SeO ₂	11.05	11.65	11.04	11.64	11.03	11.61	11.03	11.60
SiBrF ₃	11.68	12.00	11.57	11.87	11.78	12.10	11.64	11.95
SiH ₃ I	9.80	10.06	9.59	9.81	9.93	10.17	9.64	9.86
SrBr ₂	9.39	9.79	9.30	9.67	9.49	9.92	9.35	9.77
SrCl ₂	9.90	10.39	9.89	10.38	10.00	10.49	9.97	10.46
SrI ₂	8.79	9.07	8.60	8.84	8.82	9.21	8.51	8.90
TiBr ₄	9.93	10.54	9.85	10.46	9.98	10.57	9.89	10.47
TiI ₄	8.77	9.35	8.61	9.17	8.90	9.42	8.65	9.17
ZnBr ₂	10.39	10.81	10.29	10.68	10.52	10.90	10.37	10.75
ZnCl ₂	11.19	11.66	11.16	11.62	11.36	11.79	11.32	11.75
ZnF ₂	12.57	13.30	12.56	13.28	12.69	13.42	12.66	13.39
ZnI ₂	9.55	9.89	9.32	9.62	9.63	9.96	9.30	9.63
ZrBr ₄	10.20	10.75	10.15	10.67	10.26	10.78	10.17	10.68
ZrCl ₄	11.26	11.82	11.25	11.80	11.35	11.93	11.32	11.91
ZrI ₄	9.20	9.57	9.04	9.38	9.17	9.62	8.93	9.36
MSD	-0.07	-0.06	-0.04	-0.40				
MAD	0.10	0.09	0.07	0.07				
MAX	0.27	0.43	0.25	0.42				

Table 2: Comparison of the implementations of 2C- G_0W_0 in WEST and ADF/BAND.

	WEST	ADF/BAND
Single-particle basis	Plane-wave	Slater type orbital
All-electron	No	Yes
Frequency treatment	Contour deformation	Analytical continuation
QP equations	Secant method	Bisection
Relativistic Hamiltonian	2C-pseudopotentials	ZORA
2C self-energy	Static part only	Static and Dynamic part

Table 1 shows our scalar relativistic and 2C IPs using $G_0W_0@PBE$ and $G_0W_0@PBE0$ and for comparison the corresponding values from ref. 74 calculated with the WEST code. As indicated by the mean signed deviations (MSD) in table 1, ADF/BAND tends to predict lower IPs than WEST, independent of the starting point of the G_0W_0 calculation. With mean absolute deviations (MAD) of 100 meV for $G_0W_0@PBE$ and 90 meV for $G_0W_0@PBE0$ in the scalar relativistic case and of 70 meV each in the 2C case, the deviations are of the same order of magnitude as the ones we obtained for the GW100 database.^{39,135}

Several technical aspects of the *GW* implementations in ADF/BAND and WEST which are summarized in table 2 might contribute to the observed deviations. As discussed in the preceding section, these are mainly related to the different frequency treatments in both codes as well as differences in the single-particle basis. Importantly, WEST is based on PPs while we used all-electron basis sets in all ADF and BAND calculations. As already discussed extensively by Scherpelz and Govoni,⁷⁴ the choice of the PP and the partitioning of core, semi-core and valence electrons might heavily affect the values of the IPs. For instance, in ref. 74, it was shown that using different valence configurations for iodine might induce changes in IPs of the order of one eV.

In all-electron calculations, this issue is completely avoided. However, possible issues might arise from inconsistencies in the augmentation of the TZ3P and QZ6P basis sets with additional high-*l* functions. While it can be verified by comparison of TZ3P (QZ6P) results to their TZ3P+ (QZ6P+) counterparts that adding any higher angular momenta functions will improve the quality of the AO basis, the effect is typically more pronounced on the TZ than on the QZ level. This might then lead to larger inaccuracies in the CBS limit extrapolation than in plane-wave based implementations.

Changes in Ionization Potentials due to Spin-Orbit Coupling

Finally, the agreement between ADF/BAND and WEST is slightly better for the 2C than for the scalar relativistic calculations. This can be explained by the different division of scalar and spin-orbit relativistic effects in both codes (see table 2). In particular, the division between scalar relativistic and SOC effects is not unique and depends on the method of separation.¹³³

This is also illustrated by the data shown in fig. 1 where we plot the difference between the first IP in the scalar and the 2C relativistic case calculated with WEST (x-axis) against the one calculated with ADF. Overall, we find good agreement between both implementations. WEST tends to predict slightly larger shifts due to SO coupling than ADF, especially for

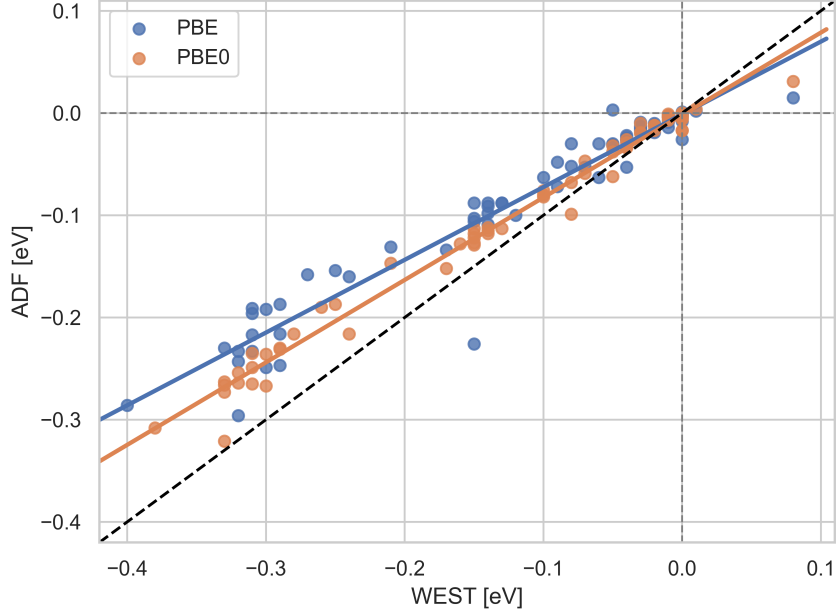


Figure 1: Comparison of the IP shift due to spin-orbit coupling as calculated with ADF compared to WEST for $G_0W_0@PBE$ and $G_0W_0@PBE0$. All values are in eV.

$G_0W_0@PBE$. This most likely indicates that ADF/BAND recovers more of the relativistic effects in the scalar relativistic treatment than WEST. At the $G_0W_0@PBE$ level we also notice one significant outlier (Cl_4) where ADF/BAND predicts significantly larger shifts due to SO coupling than WEST.

Comparison to experiment

Table 3: First ionization potentials (IP) for the SOC81* database calculated with different 2C GW methods. All values are in eV.

Name	G_0W_0			evGW ₀ @PBE0	evGW@PBE0	qsGW	exp.
	PBE	PBE0	BHLYP				
Al ₂ Br ₆	10.30	10.70	10.98	10.92	11.09	11.24	10.97
AlBr ₃	10.44	10.81	11.06	11.03	11.19	11.31	10.91
AlI ₃	9.19	9.53	9.76	9.69	9.83	9.72	9.66
AsBr ₃	9.76	10.09	10.33	10.26	10.38	10.50	10.21
AsCl ₃	10.53	10.88	11.15	11.05	11.17	11.40	10.90
AsF ₃	12.38	12.80	13.14	13.03	13.21	13.46	13.00
AsF ₅	14.47	15.30	15.81	15.74	16.13	16.62	15.53
AsH ₃	10.42	10.54	10.70	10.70	10.78	10.79	10.58
AsI ₃	8.70	9.11	9.34	9.19	9.28	9.41	9.00

Continued on next page

Name	G_0W_0			evGW ₀ @PBE0	evGW@PBE0	qsGW	exp.
	PBE	PBE0	BHLYP				
Br ₂	10.16	10.40	10.58	10.57	10.70	10.82	10.51
BrCl	10.59	10.87	11.06	11.04	11.17	11.33	11.01
C ₁₀ H ₁₀ Ru	6.83	7.12	7.44	7.24	7.43	7.87	7.45
C ₂ H ₂ Se	8.47	8.72	8.88	8.86	8.96	9.03	8.71
C ₂ H ₆ Cd	8.86	9.16	9.34	9.32	9.45	9.58	8.80
C ₂ H ₆ Hg	9.12	9.33	9.57	9.54	9.63	9.77	9.32
C ₂ H ₆ Se	8.14	8.38	8.57	8.55	8.66	8.72	8.40
C ₂ H ₆ Zn	9.42	9.70	9.89	9.89	10.04	10.10	9.40
C ₂ HBrO	9.03	9.35	9.59	9.50	9.62	9.73	9.10
C ₄ H ₄ Se	8.72	8.98	9.16	9.13	9.24	9.24	8.86
CF ₃ I	10.12	10.39	10.67	10.53	10.63	10.64	10.45
CH ₃ HgBr	9.48	9.87	10.08	10.10	10.29	10.39	10.16
CH ₃ HgCl	10.07	10.61	10.89	10.93	11.10	11.32	10.84
CH ₃ HgI	8.66	9.00	9.20	9.20	9.33	9.28	9.25
CH ₃ I	9.19	9.36	9.53	9.51	9.62	9.51	9.52
Cl ₄	8.64	9.05	9.31	9.19	9.32	9.27	9.10
CaBr ₂	9.58	9.99	10.21	10.21	10.39	10.48	10.35
CaI ₂	8.79	9.06	9.27	9.24	9.38	9.19	9.39
CdBr ₂	9.95	10.36	10.59	10.61	10.79	10.92	10.58
CdCl ₂	10.70	11.19	11.51	11.50	11.71	11.97	11.44
CdI ₂	9.06	9.36	9.57	9.54	9.69	9.61	9.57
CsF	8.49	9.50	9.79	9.91	10.32	10.60	9.68
HgCl ₂	10.61	11.02	11.30	11.28	11.48	11.85	11.50
I ₂	9.05	9.34	9.45	9.45	9.55	9.40	9.35
IBr	9.45	9.69	9.85	9.83	9.93	10.05	9.85
ICl	9.74	9.97	10.19	10.12	10.22	10.23	10.10
IF	10.14	10.34	10.56	10.48	10.60	10.57	10.62
Kr ₂	13.19	13.45	13.69	13.65	13.78	13.90	13.77
KrF ₂	12.50	13.22	13.89	13.62	13.99	14.37	13.34
LaBr ₃	9.77	10.24	10.51	10.47	10.67	10.80	10.68
LaCl ₃	10.57	11.15	11.50	11.42	11.64	11.98	11.29
LiBr	8.70	9.05	9.23	9.28	9.44	9.48	9.44
LiI	7.90	8.25	8.40	8.43	8.56	8.42	8.44
MgBr ₂	10.27	10.67	10.88	10.90	11.07	11.14	10.85
MgI ₂	9.30	9.62	9.80	9.79	9.93	9.77	10.50
MoC ₆ O ₆	8.52	8.74	9.01	8.83	8.91	9.07	8.50
OsO ₄	11.82	12.42	12.83	12.71	12.97	12.97	12.35
PBr ₃	9.54	9.86	10.11	10.01	10.13	10.27	9.99
POBr ₃	10.51	10.95	11.24	11.14	11.31	11.49	11.03
RuO ₄	11.48	12.24	12.72	12.52	12.82	13.25	12.15
SOBr ₂	10.07	10.52	10.80	10.70	10.85	11.02	10.54
SPBr ₃	9.45	9.75	10.00	9.94	10.09	10.28	9.89
SeCl ₂	9.10	9.43	9.69	9.61	9.71	10.00	9.52
SeO ₂	11.04	11.64	12.00	11.93	12.19	12.49	11.76
SiBrF ₃	11.57	11.87	12.09	12.04	12.18	12.27	12.46
SiH ₃ I	9.59	9.81	9.99	9.98	10.09	10.00	9.78
SrBr ₂	9.30	9.67	9.88	9.89	10.08	10.17	9.82
SrCl ₂	9.89	10.38	10.65	10.64	10.86	11.10	10.20
SrI ₂	8.60	8.84	9.02	9.01	9.15	9.01	9.01
TiBr ₄	9.85	10.46	10.80	10.70	10.87	11.06	10.59
TiI ₄	8.61	9.17	9.47	9.35	9.51	9.42	9.27
ZnBr ₂	10.29	10.68	10.90	10.92	11.09	11.24	10.90
ZnCl ₂	11.16	11.62	11.91	11.91	12.11	12.34	11.80

Continued on next page

Name	G_0W_0			evGW ₀ @PBE0	evGW@PBE0	qsGW	exp.
	PBE	PBE0	BHLYP				
ZnF ₂	12.56	13.28	13.72	13.85	14.30	14.73	13.91
ZnI ₂	9.32	9.62	9.83	9.81	9.94	9.87	9.76
ZrBr ₄	10.15	10.67	10.99	10.90	11.09	11.24	10.86
ZrCl ₄	11.25	11.80	12.20	12.08	12.32	12.62	11.94
ZrI ₄	9.04	9.38	9.68	9.57	9.71	9.65	9.55

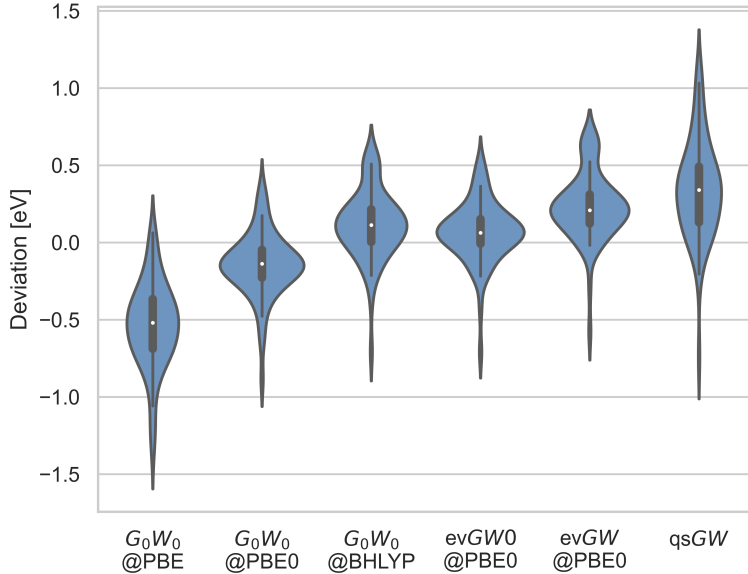


Figure 2: Distribution of the deviations of IPs (in eV) obtained with different 2C methods to the experimental reference values

In this section, we compare the different (partially self-consistent) GW variants against experimental IPs. Table 3 shows the first IPs calculated at the 2C level using (61) with six different flavors of GW : G_0W_0 based on PBE, PBE0 and BHLYP orbitals and eigenvalues (G_0W_0 @PBE, G_0W_0 @PBE0, G_0W_0 @BHLYP respectively), $evGW$ using PBE0 orbitals and eigenvalues ($evGW$ @PBE0), eigenvalue-only self-consistent GW where the screened interaction is fixed at the PBE0 level ($evGW_0$ @PBE0), and $qsGW$. MADs of all considered methods are shown in table 4. The deviations to experiment are also visualized in figure 2.

Since we take into account SO effects and since our IPs are complete basis set limit extrapolated, vertical experimental IPs are a reliable reference. Besides errors due to the technical parameters discussed in section 4, other potential sources of uncertainty are the

neglect of vibronic effects in our calculations, as well as errors in experimental geometries. Due to the lack of high-quality data from other *ab initio* calculations, these experimental reference values are however the most suitable for our purpose.

Table 4: Mean signed deviations (MSD) and mean absolute deviations (MAD) to experiment for the SOC81* set for different 1C-GW, 2C-GW and 2C-G3W2 for different starting points and different levels of partial self-consistency. All values are in eV.

		$G_0W_0@$			evGW ₀	evGW	qsGW
		PBE	PBE0	BHLYP			
MSD	1C-GW	-0.45	-0.04	0.23	0.18	0.35	0.43
	2C-GW	-0.54	-0.14	0.12	0.07	0.23	0.35
	2C-GW + G3W2	-0.46	-0.06	0.22	0.15	0.35	0.47
MAD	1C-GW	0.45	0.16	0.27	0.21	0.36	0.44
	2C-GW	0.54	0.20	0.19	0.15	0.26	0.39
	2C-GW + G3W2	0.46	0.14	0.25	0.20	0.37	0.49

Consistent with previous benchmarks on several sets of small and medium molecules,^{43,44,46,48,49,82} $G_0W_0@PBE$ greatly underestimates the first IPs. $G_0W_0@PBE0$ and $G_0W_0@BHLYP$ perform much better, with $G_0W_0@PBE0$ showing a tendency to underestimate and $G_0W_0@BHLYP$ to overestimate the experimental reference values. BHLYP contains 50 % of exact exchange which is typically about the optimal fraction for the small and medium organic molecules in the GW100 set.⁸² The good performance of $G_0W_0@PBE0$ indicates that a smaller fraction of exact exchange might be beneficial for the systems in SOC81*. This might be due to stronger screening effects in these systems containing heavy elements.

In contrast to the cited benchmark studies, evGW slightly, and qsGW more pronounced, overestimate the reference values. As shown in figure 2, qsGW is comparable with $G_0W_0@PBE$ in showing a larger spread of errors than the best performing methods. The weak performance of this method might be due to the stronger screening in the investigated systems which is typically underestimated by qsGW. This then leads to overestimated IPs and HOMO-LUMO gaps. This issue which is well documented for solids^{66,101,154-156} and it has been shown that it can be overcome by inclusion of an effective two-point kernel from time-dependent DFT or the Bethe-Salpeter equation (BSE) with a statically screened exchange kernel.¹⁵⁷⁻¹⁶⁰ Our results indicate that it might be worthwhile to explore such options also

for molecular systems.

With a MAD of 150 meV, the best performing GW method is eigenvalue-only self-consistent GW with the screened interaction kept fixed at the PBE0 level ($evGW_0@PBE0$). In an $evGW$ calculation the QP gaps increase during the iterations, leading to underestimated screening. This is compensated for by keeping the screening fixed at the PBE0 level which explains the good performance of this method. It should be noted that despite the partial self-consistency, 2C- $evGW_0$ is a particularly economic method in our implementation. The 2C polarizability is only to be evaluated once, while the self-energy, which is recalculated in each iteration, is effectively of 1C form.

Effect of the perturbative $G3W2$ correction

The perturbative inclusion of the $G3W2$ term increases the first IPs. In contrast, in ref. 49 it was shown that the $G3W2$ term tends to decrease the IPs in the ACC24 set. As shown in figure 3b), in case of $G_0W_0@PBE0$ the inclusion of this contribution improves agreement with experiment, while for $G_0W_0@BHLYP$ and the partially self-consistent methods it worsens it (figure 3c) - f)). Typically, the contribution of the $G3W2$ term to the IP is only of the order of about 0.1 eV. However, in some cases, we observe very large $G3W2$ shifts of up to 0.5 eV, for instance for RuO_4 and OsO_4 for all GW methods. This worsens agreement with experiment but their larger effect underlines the importance of vertex corrections for these systems. Out of all tested methods, with a MAD of only 140 meV, $G_0W_0@PBE0 + G3W2$ is the most accurate.

Shift of ionization potentials due to spin-orbit coupling

Generally, the SOC correction is negative, i.e. reduces the scalar relativistic IPs. This means, in case of $G_0W_0@PBE0$ the scalar relativistic results are in better agreement with experiment than the 2C ones. This is shown in figure 3b). On the other hand, for the accurate partially self-consistent approaches but also for $G_0W_0@BHLYP$, as shown in figure 3c) to figure 3e),

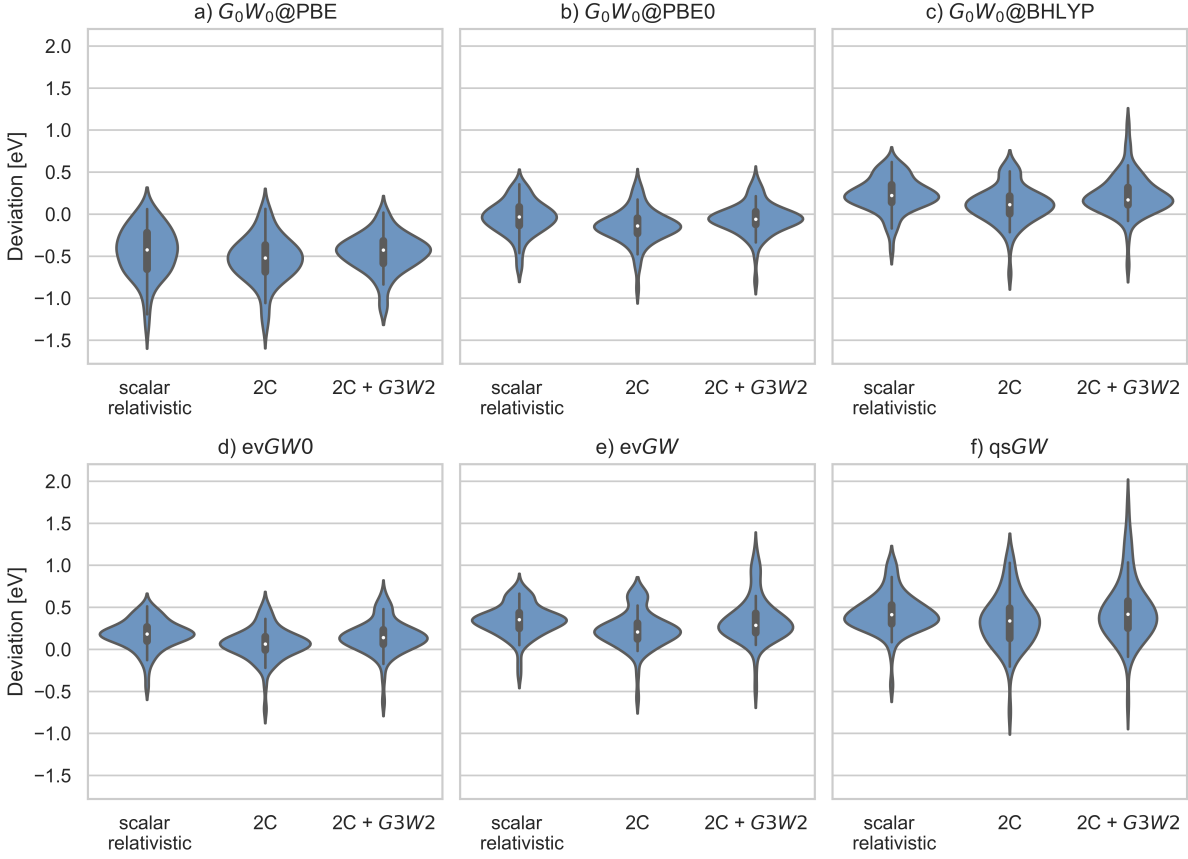


Figure 3: Distribution of the deviations to experimental reference values of IPs. Shown for each method are results for scalar relativistic, 2C and 2C calculations with perturbative $G3W2$ correction. All values are in eV.

it is crucial to take into account SOC. These observations are also reflected in the MSD and MADs shown in table 4.

Finally, in figure 4 we investigate the change in first IPs due to the explicit treatment of SOC among the different GW methods. On the x-axis, we plot the $evGW$ IPs and on the y-axis the G_0W_0 ones for different starting points. A higher amount of exact exchange in the underlying exchange-correlation functional increases the difference between the IPs at the 1C and the 2C level. The same effect as for $evGW$ can also be observed for $qsGW$ (see supporting information). This can be explained by considering the more (less) pronounced relativistic

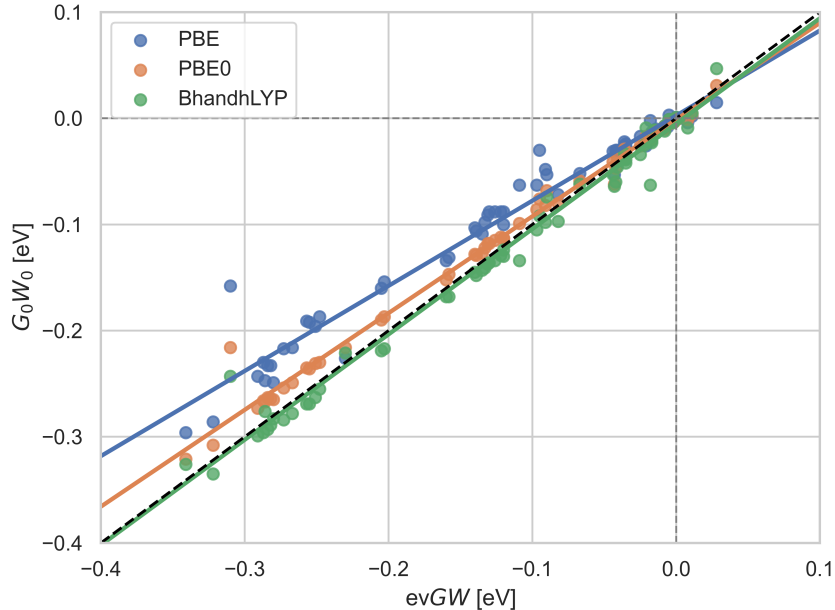


Figure 4: Differences in 2C QP energies to 1C QP energies with G_0W_0 using different starting points (x-axis) compared to $evGW$. All values are in eV.

contraction of the lower (upper) components of a degenerate orbital set that is split by the spin-orbit interaction.¹⁶¹ The ionization takes place from the upper, more diffuse, orbitals in which the exchange interaction is decreased as compared to the orbitals obtained with a scalar relativistic method. These changes in the exchange interaction induced by relativity are incompletely captured by an approximate exchange density functional approximation resulting in a too small spin-orbit splitting. Employing some non-local exchange, as done in DFT with hybrid functionals, or some form of self-consistency is required to obtain the full magnitude of this subtle effect of relativity.

5 Conclusions

We have presented an all-electron, AO based 2C implementation of the GWA for closed-shell molecules in the ADF¹²⁴ and BAND¹³⁹ engines of AMS.¹²⁵ As in our 1C GW implementation,¹⁵ we leverage the space-time formulation of the GWA, AC of the self-energy, and the PADF approximation to transform between the representations of 4-point correlation func-

tions in the AO and the auxiliary basis to achieve formally cubic scaling with system size.¹⁵ The AO-based implementation of the 2C-GWA is particularly efficient: The evaluation of the polarizability is only four times slower than in a 1C calculation. We furthermore only consider the 1-component contribution to the Green’s function to evaluate the dynamical part of the self-energy. All in all, this leads to a 2C algorithm which is only about two to three times more expensive than its 1C counterpart.

While the effect of SOC can faithfully be estimated by combining a 2C DFT calculation with a scalar relativistic *GW* calculation,⁷⁴ the new implementation will be particularly useful to calculate optical excitations within the 2C-BSE@*GW* method.

To verify the correctness of our implementation we have calculated the first IPs of a subset of 67 out of the 81 molecules in the SOC81 dataset,⁷⁴ which excludes the multi-solution cases. We have then compared our results to the ones calculated by Scherpelz and Govoni with the WEST code.⁷⁴ For scalar relativistic G_0W_0 @PBE and G_0W_0 @PBE0 first IPs, we found MADs to the WEST results of below 100 meV, respectively. With MADs of 70 meV, respectively, the agreement at the 2C level is better than in the scalar relativistic case, which can be rationalized by the different partition of scalar and spin-orbit relativistic effects in both codes. Reaching agreement between *GW* codes for molecules containing heavy elements is challenging due to relativistic effects and potentially larger errors due to incomplete single particle basis and PPs. As for the GW100 database,³⁷ further benchmark results using different types of single-particle basis, for instance Gaussian type orbitals, will be necessary to clarify the origin of the discrepancies between both codes.

Finally, we have used the new implementation to assess the accuracy of G_0W_0 based on different starting points and of partially self-consistent approaches for the first IPs of the molecules in the SOC81 set. *evGW* and *qsGW* overestimate the experimental vertical ionization energies. Especially the latter method performs poorly, which is in contrast to the good performance for small and medium, predominantly organic molecules.^{49,162} Both methods are outperformed by G_0W_0 based on PBE0 and BHLYP starting points with

fraction of 25 % and 50% of exact exchange. With a MAD of 150 meV, out of all *GW* methods the best agreement with experiment is achieved when the screened interaction is kept fixed at the PBE0 level in an eigenvalue-only self-consistent calculation (*evGW*₀@PBE0). Including SOC effects through explicit 2C calculations lowers the IPs while the inclusion of the statically screened *G3W2* correction increases them. Since *G0W0*@PBE0 alone tends to underestimate the experimental reference values, 2C-*G0W0*PBE0 + *G3W2* profits from favorable error cancellation and with a MAD of 140 meV is in excellent agreement with the experimental reference values.

In our benchmarks, we restricted ourselves to 67 out of the 81 molecules in the SOC81 benchmark set. For the other cases the non-linear QP equation (15) has multiple solutions.⁷⁴ which are difficult to describe correctly with Pade models of the frequency-dependence of the self-energy in an AC treatment. It is important to address this issue, since systems containing heavy elements, including transition metal compounds where problems with AC are ubiquitous, will be among the targets of 2C implementations. AC can be avoided by using analytical integration of the self-energy^{8,150,151} or contour deformation techniques.^{21,50,74,152} AC of the screened interaction can also be combined with CD of the self-energy^{153,163} to compute a single-matrix element of the self-energy in the MO basis with cubic scaling with system size. This technique is therefore suitable for *G0W0* and also for *evGW* or *BSE@GW* calculations where Hedin shifts^{54,164} or other rigid scissor-like shifts of the KS spectrum^{19,75,165} can be employed to avoid the explicit calculation of all diagonal elements of the self-energy. Since in *qsGW* the full self-energy matrix is needed, such an algorithm would scale as $\mathcal{O}(N^5)$ with system size and is therefore only suitable for small molecules. Together with the already mentioned convergence problems as well as the generally poor performance for the systems considered herein, this is in principle a strong argument against the use of *qsGW* for such systems.

A Proof of Eqs. 29 and 30

In this appendix we proof eqs. (27) and (28), which are valid under Kramers symmetry. We employ relation eq. (19) to first proof (28). In real space,

$$\begin{aligned}
P^{(0)}(\mathbf{r} \uparrow, \mathbf{r}' \uparrow, i\tau) &= -i \sum_{ia} e^{-(\epsilon_a - \epsilon_i)\tau} \phi_i^\uparrow(\mathbf{r}) \phi_i^{\uparrow*}(\mathbf{r}') \phi_a^\uparrow(\mathbf{r}') \phi_a^{\uparrow*}(\mathbf{r}) \\
&= -i \sum_{ia} e^{-(\epsilon_a - \epsilon_i)\tau} \phi_i^{\downarrow*}(\mathbf{r}) \phi_i^\downarrow(\mathbf{r}') \phi_a^{\downarrow*}(\mathbf{r}') \phi_a^\downarrow(\mathbf{r}) \\
&= P^{(0)}(\mathbf{r}' \downarrow, \mathbf{r} \downarrow, i\tau) = P^{(0)}(\mathbf{r} \downarrow, \mathbf{r}' \downarrow, i\tau)
\end{aligned} \tag{65}$$

with the last equality due to the symmetry of $P^{(0)}$. In the same way, we also show the identity

$$\begin{aligned}
P^{(0)}(\mathbf{r} \uparrow, \mathbf{r}' \downarrow, i\tau) &= -i \sum_{ia} e^{-(\epsilon_a - \epsilon_i)\tau} \phi_i^\uparrow(\mathbf{r}) \phi_i^{\downarrow*}(\mathbf{r}') \phi_a^\downarrow(\mathbf{r}') \phi_a^{\uparrow*}(\mathbf{r}) \\
&= -i \sum_{ia} e^{-(\epsilon_a - \epsilon_i)\tau} \phi_i^{\downarrow*}(\mathbf{r}) \phi_i^\uparrow(\mathbf{r}') \phi_a^{\uparrow*}(\mathbf{r}') \phi_a^\downarrow(\mathbf{r}) \\
&= P^{(0)}(\mathbf{r}' \uparrow, \mathbf{r} \downarrow, i\tau) = P^{(0)}(\mathbf{r} \downarrow, \mathbf{r}' \uparrow, i\tau).
\end{aligned} \tag{66}$$

After transformation to the AO basis, these are the identities in (28).

Equation (27),

$$\sum_{\sigma, \sigma' = \uparrow, \downarrow} iG_{\mu\kappa, \sigma\sigma'}^{>I}(i\tau) G_{\nu\lambda, \sigma'\sigma}^{<R}(-i\tau) + iG_{\mu\kappa, \sigma\sigma'}^{>R}(i\tau) G_{\nu\lambda, \sigma'\sigma}^{<I}(-i\tau) = 0. \tag{67}$$

follows from the cancellation of terms in the sums due to the identities

$$G_{\mu\kappa, \uparrow\uparrow}^{>I}(i\tau) G_{\nu\lambda, \uparrow\uparrow}^{<R}(-i\tau) = -G_{\mu\kappa, \downarrow\downarrow}^{>I}(i\tau) G_{\nu\lambda, \downarrow\downarrow}^{<R}(-i\tau) \tag{68}$$

$$G_{\mu\kappa, \uparrow\uparrow}^{>R}(i\tau) G_{\nu\lambda, \uparrow\uparrow}^{<I}(-i\tau) = -G_{\mu\kappa, \downarrow\downarrow}^{>R}(i\tau) G_{\nu\lambda, \downarrow\downarrow}^{<I}(-i\tau) \tag{69}$$

$$G_{\mu\kappa, \uparrow\downarrow}^{>I}(i\tau) G_{\nu\lambda, \downarrow\uparrow}^{<R}(-i\tau) = -G_{\mu\kappa, \downarrow\uparrow}^{>I}(i\tau) G_{\nu\lambda, \uparrow\downarrow}^{<R}(-i\tau) \tag{70}$$

$$G_{\mu\kappa, \uparrow\downarrow}^{>R}(i\tau) G_{\nu\lambda, \downarrow\uparrow}^{<I}(-i\tau) = -G_{\mu\kappa, \downarrow\uparrow}^{>R}(i\tau) G_{\nu\lambda, \uparrow\downarrow}^{<I}(-i\tau), \tag{71}$$

These relations follow directly from eq. (24), as in each of the four terms there is exactly one

sign change upon applying Kramers’ symmetry.

B Computational timings

Table 5: Computational timings and first IP of Ir(ppy)₃ for different basis sets at the 1C and 2C level using $G_0W_0@PBE0$.

		TZ3P		QZ6P	
		1C	2C	1C	2C
N_{bas}		1566		2895	
Total	[core h]	41	82	728	1995
$P^{(0)}$	[core h]	14	53	409	1655
W	[core h]	4	4	30	30
Σ	[core h]	21	20	205	213
first IP	[eV]	6.09	5.81	6.13	5.78

In this appendix we compare the computational timings of 1C and 2C GW calculations in our implementation. We report here timings for Tris(2-phenylpyridine)iridium [Ir(ppy)₃], a molecule with 320 electrons which is widely used in organic light-emitting diodes (OLEDs) due to its high quantum yields, enabled by thermally activated delayed fluorescence (TADF).¹⁶⁶ Timing results for the full complex at the TZ3P and QZ6P level using the ADF engine are shown in table 5. Systems like Ir(ppy)₃ which contain many first- and second-row atoms are suitable for AO-based implementations since they can exploit sparsity in the AO basis. For clusters of heavy elements, for instance the Pb₁₄Se₁₃ cluster considered in ref. 74, MO-based implementations are more suitable, even though their asymptotic scaling with system size is less favorable.

As one would expect from the equations in section 2, independently of the basis set the calculation of the polarizability is four times slower in the 2C case, while the timings for the other most time-consuming parts of a G_0W_0 calculation remain the same. In the QZ calculations, the timings are dominated by the calculation of the polarizability and therefore the 2C calculation is slower compared to the 1C calculation than for the TZ calculations. A single iteration of a partially self-consistent calculation (both $evGW$ and $qsGW$) is as

time-consuming as a G_0W_0 calculation. An $evGW_0$ calculation is more economic as a $evGW$ calculation, since the polarizability needs to be evaluated only once, saving about a factor of 2 in each iteration.

Acknowledgement

Edoardo Spadetto acknowledges funding from the European Union's Horizon 2020 research and innovation program under grant agreement No 956813 (2Exciting).

Supporting Information Available

All Quasiparticle energies calculated in this work. All basis set files.

References

- (1) Hedin, L. New method for calculating the one-particle Green's function with application to the electron-gas problem. *Phys. Rev.* **1965**, *139*, A796.
- (2) Martin, R. M.; Reining, L.; Ceperley, D. M. *Interacting electrons*; Cambridge University Press, 2016.
- (3) Reining, L. The GW approximation: content, successes and limitations. *Wiley Interdiscip. Rev. Comput. Mol. Sci.* **2018**, *8*, e1344.
- (4) Golze, D.; Dvorak, M.; Rinke, P. The GW Compendium: A Practical Guide to Theoretical Photoemission Spectroscopy. *Front. Chem.* **2019**, *7*, 377.
- (5) Ren, X.; Rinke, P.; Blum, V.; Wieferink, J.; Tkatchenko, A.; Sanfilippo, A.; Reuter, K.; Scheffler, M. Resolution-of-identity approach to Hartree-Fock, hybrid density functionals, RPA, MP2 and GW with numeric atom-centered orbital basis functions. *New J. Phys.* **2012**, *14*, 053020.

- (6) Caruso, F.; Rinke, P.; Ren, X.; Scheffler, M.; Rubio, A. Unified description of ground and excited states of finite systems: The self-consistent GW approach. *Phys. Rev. B* **2012**, *86*, 081102(R).
- (7) Caruso, F.; Rinke, P.; Ren, X.; Rubio, A.; Scheffler, M. Self-consistent GW: All-electron implementation with localized basis functions. *Phys. Rev. B* **2013**, *88*, 075105.
- (8) Van Setten, M. J.; Weigend, F.; Evers, F. The GW-method for quantum chemistry applications: Theory and implementation. *J. Chem. Theory Comput.* **2013**, *9*, 232–246.
- (9) Kaplan, F.; Weigend, F.; Evers, F.; Van Setten, M. J. Off-diagonal self-energy terms and partially self-consistency in GW calculations for single molecules: Efficient implementation and quantitative effects on ionization potentials. *J. Chem. Theory Comput.* **2015**, *11*, 5152–5160.
- (10) Kaplan, F.; Harding, M. E.; Seiler, C.; Weigend, F.; Evers, F.; Van Setten, M. J. Quasi-Particle Self-Consistent GW for Molecules. *J. Chem. Theory Comput.* **2016**, *12*, 2528–2541.
- (11) Bruneval, F.; Rangel, T.; Hamed, S. M.; Shao, M.; Yang, C.; Neaton, J. B. MOLGW 1: Many-body perturbation theory software for atoms, molecules, and clusters. *Comput. Phys. Commun.* **2016**, *208*, 149–161.
- (12) Foerster, D.; Koval, P.; Snchez-Portal, D. An $O(N^3)$ implementation of Hedin's GW approximation for molecules. *J. Chem. Phys.* **2011**, *135*, 074105.
- (13) Koval, P.; Foerster, D.; Sánchez-Portal, D. Fully self-consistent GW and quasiparticle self-consistent GW for molecules. *Phys. Rev. B* **2014**, *89*, 155417.
- (14) Mejia-Rodriguez, D.; Kunitsa, A.; Aprà, E.; Govind, N. Scalable Molecular GW Calculations: Valence and Core Spectra. *J. Chem. Theory Comput.* **2021**, *17*, 7504–7517.

- (15) Förster, A.; Visscher, L. Low-Order Scaling G0W0 by Pair Atomic Density Fitting. *J. Chem. Theory Comput.* **2020**, *16*, 7381–7399.
- (16) Förster, A.; Visscher, L. Low-Order Scaling Quasiparticle Self-Consistent GW for Molecules. *Front. Chem.* **2021**, *9*, 736591.
- (17) Wilhelm, J.; Del Ben, M.; Hutter, J. GW in the Gaussian and Plane Waves Scheme with Application to Linear Acenes. *J. Chem. Theory Comput.* **2016**, *12*, 3623–3635.
- (18) Wilhelm, J.; Golze, D.; Talirz, L.; Hutter, J.; Pignedoli, C. A. Toward GW Calculations on Thousands of Atoms. *J. Phys. Chem. Lett.* **2018**, *9*, 306–312.
- (19) Wilhelm, J.; Seewald, P.; Golze, D. Low-scaling GW with benchmark accuracy and application to phosphorene nanosheets. *J. Chem. Theory Comput.* **2021**, *17*, 1662–1677.
- (20) Ke, S. H. All-electron GW methods implemented in molecular orbital space: Ionization energy and electron affinity of conjugated molecules. *Phys. Rev. B* **2011**, *84*, 205415.
- (21) Govoni, M.; Galli, G. Large Scale GW Calculations. *J. Chem. Theory Comput.* **2015**, *11*, 2680–2696.
- (22) Del Ben, M.; da Jornada, F. H.; Canning, A.; Wichmann, N.; Raman, K.; Sasanka, R.; Yang, C.; Louie, S. G.; Deslippe, J. Large-scale GW calculations on pre-exascale HPC systems. *Comput. Phys. Commun.* **2019**, *235*, 187–195.
- (23) Del Ben, M.; da Jornada, F. H.; Antonius, G.; Rangel, T.; Louie, S. G.; Deslippe, J.; Canning, A. Static subspace approximation for the evaluation of G0W0 quasiparticle energies within a sum-over-bands approach. *Phys. Rev. B* **2019**, *99*, 125128.
- (24) Yu, V. W. Z.; Govoni, M. GPU Acceleration of Large-Scale Full-Frequency GW Calculations. *J. Chem. Theory Comput.* **2022**, *18*, 4690–4707.

- (25) Duchemin, I.; Blase, X. Cubic-Scaling All-Electron GW Calculations with a Separable Density-Fitting Space-Time Approach. *J. Chem. Theory Comput.* **2021**, *17*, 2383–2393.
- (26) Vlček, V.; Rabani, E.; Neuhauser, D.; Baer, R. Stochastic GW Calculations for Molecules. *J. Chem. Theory Comput.* **2017**, *13*, 4997–5003.
- (27) Vlček, V.; Li, W.; Baer, R.; Rabani, E.; Neuhauser, D. Swift GW beyond 10,000 electrons using sparse stochastic compression. *Phys. Rev. B* **2018**, *98*, 075107.
- (28) Fujita, T.; Noguchi, Y. Development of the fragment-based COHSEX method for large and complex molecular systems. *Phys. Rev. B* **2018**, *98*, 205140.
- (29) Fujita, T.; Noguchi, Y.; Hoshi, T. Charge-transfer excited states in the donor/acceptor interface from large-scale GW calculations. *J. Chem. Phys.* **2019**, *151*, 114109.
- (30) Winter, M.; Bousquet, M. H. E.; Jacquemin, D.; Duchemin, I.; Blase, X. Photoluminescent properties of the carbon-dimer defect in hexagonal boron-nitride: A many-body finite-size cluster approach. *Phys. Rev. Mater.* **2021**, *5*, 95201.
- (31) Amblard, D.; D’avino, G.; Duchemin, I.; Blase, X. Universal polarization energies for defects in monolayer, surface, and bulk hexagonal boron nitride: A finite-size fragments GW approach. *Phys. Rev. Mater.* **2022**, *6*, 064008.
- (32) Romanova, M.; Vlček, V. Decomposition and embedding in the stochastic GW self-energy. *J. Chem. Phys.* **2020**, *153*, 134103.
- (33) Weng, G.; Vlček, V. Efficient treatment of molecular excitations in the liquid phase environment via stochastic many-body theory. *J. Chem. Phys.* **2021**, *155*, 054104.
- (34) Tölle, J.; Deilmann, T.; Rohl, M.; Neugebauer, J. Subsystem-Based GW / Bethe - Salpeter Equation. *J. Chem. Theory Comput.* **2021**, *17*, 2186–2199.

- (35) Förster, A.; Visscher, L. Quasiparticle Self-Consistent GW-Bethe-Salpeter equation calculations for large chromophoric systems. *J. Chem. Theory Comput.* **2022**, *18*, 6779–6793.
- (36) Borin Barin, G.; Sun, Q.; Di Giovannantonio, M.; Du, C. Z.; Wang, X. Y.; Llinas, J. P.; Mutlu, Z.; Lin, Y.; Wilhelm, J.; Overbeck, J.; Daniels, C.; Lamparski, M.; Sahabudeen, H.; Perrin, M. L.; Urgel, J. I.; Mishra, S.; Kinikar, A.; Widmer, R.; Stolz, S.; Bommert, M.; Pignedoli, C.; Feng, X.; Calame, M.; Müllen, K.; Narita, A.; Meunier, V.; Bokor, J.; Fasel, R.; Ruffieux, P. Growth Optimization and Device Integration of Narrow-Bandgap Graphene Nanoribbons. *Small* **2022**, *18*, 2202301.
- (37) Van Setten, M. J.; Caruso, F.; Sharifzadeh, S.; Ren, X.; Scheffler, M.; Liu, F.; Lischner, J.; Lin, L.; Deslippe, J. R.; Louie, S. G.; Yang, C.; Weigend, F.; Neaton, J. B.; Evers, F.; Rinke, P. GW100: Benchmarking G0W0 for Molecular Systems. *J. Chem. Theory Comput.* **2015**, *11*, 5665–5687.
- (38) Maggio, E.; Kresse, G. Correlation energy for the homogeneous electron gas: Exact Bethe-Salpeter solution and an approximate evaluation. *Phys. Rev. B* **2016**, *93*, 235113.
- (39) Govoni, M.; Galli, G. GW100: Comparison of Methods and Accuracy of Results Obtained with the WEST Code. *J. Chem. Theory Comput.* **2018**, *14*, 1895–1909.
- (40) Gao, W.; Chelikowsky, J. R. Real-Space Based Benchmark of G0W0 Calculations on GW100: Effects of Semicore Orbitals and Orbital Reordering. *J. Chem. Theory Comput.* **2019**, *15*, 5299–5307.
- (41) Bruneval, F.; Maliyov, I.; Lapointe, C.; Marinica, M.-C. Extrapolating unconverged GW energies up to the complete basis set limit with linear regression. *J. Chem. Theory Comput.* **2020**, *16*, 4399–4407.

- (42) Bruneval, F. GW approximation of the many-body problem and changes in the particle number. *Phys. Rev. Lett.* **2009**, *103*, 1–4.
- (43) Marom, N.; Caruso, F.; Ren, X.; Hofmann, O. T.; Körzdörfer, T.; Chelikowsky, J. R.; Rubio, A.; Scheffler, M.; Rinke, P. Benchmark of GW methods for azabenzenes. *Phys. Rev. B* **2012**, *86*, 245127.
- (44) Bruneval, F.; Marques, M. Benchmarking the starting points of the GW approximation for molecules. *J. Chem. Theory Comput.* **2013**, *9*, 324–329.
- (45) Ren, X.; Marom, N.; Caruso, F.; Scheffler, M.; Rinke, P. Beyond the GW approximation: A second-order screened exchange correction. *Phys. Rev. B - Condens. Matter Mater. Phys.* **2015**, *92*, 081104(R).
- (46) Knight, J. W.; Wang, X.; Gallandi, L.; Dolgounitcheva, O.; Ren, X.; Ortiz, J. V.; Rinke, P.; Körzdörfer, T.; Marom, N. Accurate Ionization Potentials and Electron Affinities of Acceptor Molecules III: A Benchmark of GW Methods. *J. Chem. Theory Comput.* **2016**, *12*, 615–626.
- (47) Rangel, T.; Hamed, S. M.; Bruneval, F.; Neaton, J. B. Evaluating the GW Approximation with CCSD(T) for Charged Excitations Across the Oligoacenes. *J. Chem. Theory Comput.* **2016**, *12*, 2834–2842.
- (48) Caruso, F.; Dauth, M.; Van Setten, M. J.; Rinke, P. Benchmark of GW Approaches for the GW100 Test Set. *J. Chem. Theory Comput.* **2016**, *12*, 5076–5087.
- (49) Förster, A.; Visscher, L. Exploring the statically screened G3W2 correction to the GW self-energy : Charged excitations and total energies of finite systems. *Phys. Rev. B* **2022**, *105*, 125121.
- (50) Golze, D.; Wilhelm, J.; Van Setten, M. J.; Rinke, P. Core-Level Binding Energies

- from GW: An Efficient Full-Frequency Approach within a Localized Basis. *J. Chem. Theory Comput.* **2018**, *14*, 4856–4869.
- (51) Van Setten, M. J.; Costa, R.; Viñes, F.; Illas, F. Assessing GW Approaches for Predicting Core Level Binding Energies. *J. Chem. Theory Comput.* **2018**, *14*, 877–883.
- (52) Golze, D.; Keller, L.; Rinke, P. Accurate Absolute and Relative Core-Level Binding Energies From GW. *J. Phys. Chem. Lett.* **2020**, *11*, 1840–1847.
- (53) Yao, Y.; Golze, D.; Rinke, P.; Blum, V.; Kanai, Y. All-Electron BSE@ GW Method for K -Edge Core Electron Excitation Energies. *J. Chem. Theory Comput.* **2022**, *18*, 1569–1583.
- (54) Li, J.; Jin, Y.; Rinke, P.; Yang, W.; Golze, D. Benchmark of GW Methods for Core-Level Binding Energies. *J. Chem. Theory Comput.* **2022**, *18*, 7570–7585.
- (55) Mansouri, M.; Casanova, D.; Koval, P.; Sánchez-Portal, D. GW approximation for open-shell molecules: A first-principles study. *New J. Phys.* **2021**, *23*.
- (56) Körbel, S.; Boulanger, P.; Duchemin, I.; Blase, X.; Marques, M.; Botti, S. Benchmark many-body GW and Bethe-Salpeter calculations for small transition metal molecules. *J. Chem. Theory Comput.* **2014**, *10*, 3934–3943.
- (57) Berardo, E.; Kaplan, F.; Bhaskaran-Nair, K.; Shelton, W. A.; Van Setten, M. J.; Kowalski, K.; Zwijnenburg, M. A. Benchmarking the Fundamental Electronic Properties of small TiO₂ Nanoclusters by GW and Coupled Cluster Theory Calculations. *J. Chem. Theory Comput.* **2017**, *13*, 3814–3828.
- (58) Hung, L.; Bruneval, F.; Baishya, K.; Ögüt, S. Benchmarking the GW Approximation and Bethe-Salpeter Equation for Groups IB and IIB Atoms and Monoxides. *J. Chem. Theory Comput.* **2017**, *13*, 2135–2146.

- (59) Shi, B.; Weissman, S.; Bruneval, F.; Kronik, L.; Ögüt, S. Photoelectron spectra of copper oxide cluster anions from first principles methods. *J. Chem. Phys.* **2018**, *149*, 064306.
- (60) Byun, Y.-m.; Ögüt, S. Practical GW scheme for electronic structure of 3 d-transition-metal monoxide anions : ScO-, TiO-, CuO-, and ZnO-. *J. Chem. Phys.* **2019**, *151*, 134305.
- (61) Rezaei, M.; Ögüt, S. Photoelectron spectra of early 3d-transition metal dioxide molecular anions from GW calculations. *J. Chem. Phys.* **2021**, *154*, 094307.
- (62) Wang, X.; Gao, S.; Zhao, M.; Marom, N. Benchmarking time-dependent density functional theory for singlet excited states of thermally activated delayed fluorescence chromophores. *Phys. Rev. Res.* **2022**, *4*, 033147.
- (63) Hybertsen, M. S.; Louie, S. G. First-principles theory of quasiparticles: Calculation of band gaps in semiconductors and insulators. *Phys. Rev. Lett.* **1985**, *55*, 1418–1421.
- (64) Hybertsen, M. S.; Louie, S. G. Electron correlation in semiconductors and insulators: Band gaps and quasiparticle energies. *Phys. Rev. B* **1986**, *34*, 5390.
- (65) Faleev, S. V.; van Schilfgaarde, M.; Kotani, T. All-electron self-consistent GW approximation: Application to Si, MnO, and NiO. *Phys. Rev. Lett.* **2004**, *93*, 126406.
- (66) van Schilfgaarde, M.; Kotani, T.; Faleev, S. Quasiparticle self-consistent GW theory. *Phys. Rev. Lett.* **2006**, *96*, 226402.
- (67) Kotani, T.; van Schilfgaarde, M.; Faleev, S. V. Quasiparticle self-consistent GW method: A basis for the independent-particle approximation. *Phys. Rev. B* **2007**, *76*, 165106.
- (68) Gui, X.; Holzer, C.; Klopper, W. Accuracy Assessment of GW Starting Points for

- Calculating Molecular Excitation Energies Using the Bethe-Salpeter Formalism. *J. Chem. Theory Comput.* **2018**, *14*, 2127–2136.
- (69) Akinaga, Y.; Nakajima, T. Two-component relativistic equation-of-motion coupled-cluster methods for excitation energies and ionization potentials of atoms and molecules. *J. Phys. Chem. A* **2017**, *121*, 827–835.
- (70) Shee, A.; Saue, T.; Visscher, L.; Severo Pereira Gomes, A. Equation-of-motion coupled-cluster theory based on the 4-component Dirac-Coulomb(-Gaunt) Hamiltonian. Energies for single electron detachment, attachment, and electronically excited states. *J. Chem. Phys.* **2018**, *149*.
- (71) Aryasetiawan, F.; Biermann, S. Generalized Hedin’s equations for quantum many-body systems with spin-dependent interactions. *Phys. Rev. Lett.* **2008**, *100*, 116402.
- (72) Aryasetiawan, F.; Biermann, S. Generalized Hedin equations and $\sigma\sigma W$ approximation for quantum many-body systems with spin-dependent interactions. *J. Phys. Condens. Matter* **2009**, *21*, 6–9.
- (73) Kühn, M.; Weigend, F. One-electron energies from the two-component GW method. *J. Chem. Theory Comput.* **2015**, *11*, 969–979.
- (74) Scherpelz, P.; Govoni, M.; Hamada, I.; Galli, G. Implementation and Validation of Fully Relativistic GW Calculations: Spin-Orbit Coupling in Molecules, Nanocrystals, and Solids. *J. Chem. Theory Comput.* **2016**, *12*, 3523–3544.
- (75) Holzer, C.; Klopper, W. Ionized, electron-attached, and excited states of molecular systems with spin-orbit coupling: Two-component GW and Bethe-Salpeter implementations. *J. Chem. Phys.* **2019**, *150*, 204116.
- (76) Franzke, Y. J.; Holzer, C.; Mack, F. NMR Coupling Constants Based on the Bethe-

- Salpeter Equation in the GW Approximation. *J. Chem. Theory Comput.* **2022**, *18*, 1030–1045.
- (77) Holzer, C. Practical post-Kohn – Sham methods for time-reversal symmetry breaking references. *ChemRxiv* **2023**, 1–42.
- (78) Perdew, J. P.; Burke, K.; Ernzerhof, M. Generalized gradient approximation made simple. *Phys. Rev. Lett.* **1996**, *77*, 3865–3868.
- (79) Adamo, C.; Barone, V. Toward reliable density functional methods without adjustable parameters: The PBE0 model. *J. Chem. Phys.* **1999**, *110*, 6158–6170.
- (80) Ernzerhof, M.; Scuseria, G. E. Assessment of the Perdew–Burke–Ernzerhof exchange–correlation functional. *J. Chem. Phys.* **1999**, *110*, 5029.
- (81) Wang, Y.; Rinke, P.; Ren, X. Assessing the $G_0W_0\Gamma_0(1)$ Approach: Beyond G_0W_0 with Hedin’s Full Second-Order Self-Energy Contribution. *J. Chem. Theory Comput.* **2021**, *17*, 5140–5154.
- (82) Zhang, L.; Shu, Y.; Xing, C.; Chen, X.; Sun, S.; Huang, Y.; Truhlar, D. G. Recommendation of Orbitals for G_0W_0 Calculations on Molecules and Crystals. *J. Chem. Theory Comput.* **2022**, *18*, 3523–3537.
- (83) Ma, H.; Govoni, M.; Gygi, F.; Galli, G. A Finite-Field Approach for GW Calculations beyond the Random Phase Approximation. *J. Chem. Theory Comput.* **2019**, *15*, 154–164.
- (84) Vlček, V. Stochastic Vertex Corrections: Linear Scaling Methods for Accurate Quasi-particle Energies. *J. Chem. Theory Comput.* **2019**, *15*, 6254–6266.
- (85) Pavlyukh, Y.; Stefanucci, G.; van Leeuwen, R. Dynamically screened vertex correction to GW. *Phys. Rev. B* **2020**, *102*, 045121.

- (86) Bruneval, F.; Dattani, N.; van Setten, M. J. The GW Miracle in Many-Body Perturbation Theory for the Ionization Potential of Molecules. *Front. Chem.* **2021**, *9*, 749779.
- (87) Wang, Y.; Ren, X. Vertex effects in describing the ionization energies of the first-row transition-metal monoxide molecules. *J. Chem. Phys.* **2022**, *157*, 214115.
- (88) Mejuto-Zaera, C.; Vlček, V. Self-consistency in GW Γ formalism leading to quasiparticle-quasiparticle couplings. *Phys. Rev. B* **2022**, *106*, 165129.
- (89) Kutepov, A. L.; Kotliar, G. One-electron spectra and susceptibilities of the three-dimensional electron gas from self-consistent solutions of Hedin's equations. *Phys. Rev. B* **2017**, *96*, 035108.
- (90) Kutepov, A. L. Self-consistent solution of Hedin's equations: Semiconductors and insulators. *Phys. Rev. B* **2017**, *95*, 195120.
- (91) Förster, A. Assessment of the second-order statically screened exchange correction to the random phase approximation for correlation energies. *J. Chem. Theory Comput.* **2022**, *18*, 5948–5965.
- (92) Rieger, M. M.; Steinbeck, L.; White, I. D.; Rojas, H. N.; Godby, R. W. GW space-time method for the self-energy of large systems. *Comput. Phys. Commun.* **1999**, *117*, 211–228.
- (93) Hohenberg, P.; Kohn, W. Inhomogeneous Electron Gas. *Phys. Rev.* **1964**, *136*, 864–871.
- (94) Kohn, W.; Sham, L. J., Self-Consistent Equations Including Exchange and Correlation Effects. *Phys. Rev.* **1965**, *140*, A1133.
- (95) Seidl, A.; Görling, A.; Vogl, P.; Majewski, J.; Levy, M. Generalized Kohn-Sham schemes and the band-gap problem. *Phys. Rev. B* **1996**, *53*, 3764–3774.

- (96) Layzer, A. J. Properties of the one-particle green's function for nonuniform many-fermion systems. *Phys. Rev.* **1963**, *129*, 897–907.
- (97) Sham, L. J.; Kohn, W. One-particle properties of an inhomogeneous interacting electron gas. *Phys. Rev.* **1966**, *145*, 561–567.
- (98) Hüser, F.; Olsen, T.; Thygesen, K. S. Quasiparticle GW calculations for solids, molecules, and two-dimensional materials. *Phys. Rev. B - Condens. Matter Mater. Phys.* **2013**, *87*, 235132.
- (99) Nakashima, T.; Raebiger, H.; Ohno, K. Normalization of exact quasiparticle wave functions in the Green ' s function method guaranteed by the Ward identity. *Phys. Rev. B* **2021**, *104*, L201116.
- (100) It should be understood that in practice one solves

$$\sum_q \left\{ [\Sigma_{Hxc}^H]_{pq} - [\Sigma_{Hxc}^{H^{(n-1)}}]_{pq} \right\} \phi_q(\mathbf{r}) = (\epsilon_p - \epsilon_p^{(n-1)}) \phi_p(\mathbf{r}) \quad (72)$$

in the n th iteration, which reduces to (16) for $n = 1$.

- (101) Shishkin, M.; Marsman, M.; Kresse, G. Accurate quasiparticle spectra from self-consistent GW calculations with vertex corrections. *Phys. Rev. Lett.* **2007**, *99*, 246403.
- (102) Kutepov, A.; Haule, K.; Savrasov, S. Y.; Kotliar, G. Electronic structure of Pu and Am metals by self-consistent relativistic GW method. *Phys. Rev. B - Condens. Matter Mater. Phys.* **2012**, *85*, 155129.
- (103) Kutepov, A. L.; Oudovenko, V. S.; Kotliar, G. Linearized self-consistent quasiparticle GW method: Application to semiconductors and simple metals. *Comput. Phys. Commun.* **2017**, *219*, 407–414.
- (104) Friedrich, C.; Blügel, S.; Nabok, D. Quasiparticle Self-Consistent GW Study of Simple Metals. *Nanomaterials* **2022**, *12*.

- (105) Lei, J.; Zhu, T. Gaussian-based quasiparticle self-consistent GW for periodic systems. *J. Chem. Phys.* **2022**, *157*, 214114.
- (106) Saue, T.; Jensen, H. J. Quaternion symmetry in relativistic molecular calculations: The Dirac-Hartree-Fock method. *J. Chem. Phys.* **1999**, *111*, 6211–6222.
- (107) Sakuma, R.; Friedrich, C.; Miyake, T.; Blügel, S.; Aryasetiawan, F. GW calculations including spin-orbit coupling: Application to Hg chalcogenides. *Phys. Rev. B - Condens. Matter Mater. Phys.* **2011**, *84*, 1–10.
- (108) Watson, M. A.; Handy, N. C.; Cohen, A. J. Density functional calculations, using Slater basis sets, with exact exchange. *J. Chem. Phys.* **2003**, *119*, 6475–6481.
- (109) Krykunov, M.; Ziegler, T.; Van Lenthe, E. Hybrid density functional calculations of nuclear magnetic shieldings using slater-type orbitals and the zeroth-order regular approximation. *Int. J. Quantum Chem.* **2009**, *109*, 1676–1683.
- (110) Merlot, P.; Kjærgaard, T.; Helgaker, T.; Lindh, R.; Aquilante, F.; Reine, S.; Pedersen, T. B. Attractive electron-electron interactions within robust local fitting approximations. *J. Comput. Chem.* **2013**, *34*, 1486–1496.
- (111) Merlot, P.; Izsák, R.; Borgoo, A.; Kjærgaard, T.; Helgaker, T.; Reine, S. Charge-constrained auxiliary-density-matrix methods for the Hartree-Fock exchange contribution. *J. Chem. Phys.* **2014**, *141*, 094104.
- (112) Wirz, L. N.; Reine, S. S.; Pedersen, T. B. On Resolution-of-the-Identity Electron Repulsion Integral Approximations and Variational Stability. *J. Chem. Theory Comput.* **2017**, *13*, 4897–4906.
- (113) Ihrig, A. C.; Wieferink, J.; Zhang, I. Y.; Ropo, M.; Ren, X.; Rinke, P.; Scheffler, M.; Blum, V. Accurate localized resolution of identity approach for linear-scaling hybrid

- density functionals and for many-body perturbation theory. *New J. Phys.* **2015**, *17*, 093020.
- (114) Spadetto, E.; Philipsen, P. H. T.; Förster, A.; Visscher, L. Toward Pair Atomic Density Fitting for Correlation Energies with Benchmark Accuracy. *J. Chem. Theory Comput.* **2023**, *19*, 1499–1516.
- (115) Dunlap, B. I.; Connolly, J. W.; Sabin, J. R. On some approximations in applications of $X\alpha$ theory. *J. Chem. Phys.* **1979**, *71*, 3396–3402.
- (116) Feyereisen, M.; Fitzgerald, G.; Komornicki, A. Use of approximate integrals in ab initio theory. An application in MP2 energy calculations. *Chem. Phys. Lett.* **1993**, *208*, 359–363.
- (117) Jung, Y.; Sodt, A.; Gill, P. M. W.; Head-Gordon, M. Auxiliary basis expansions for large-scale electronic structure calculations. *Proc. Natl. Acad. Sci.* **2005**, *102*, 6692–6697.
- (118) van Leeuwen, R.; Dahlen, N. E.; Stefanucci, G.; Almladh, C. O.; Von Barth, U. In *Time-Dependent Density Funct. Theory*; Marques, M. A., Ullrich, C. A., Nogueira, F., Rubio, A., Burke, K., Gross, E. K., Eds.; Springer Heidelberg, 2015; pp 185–217.
- (119) Liu, P.; Kaltak, M.; Klimeš, J.; Kresse, G. Cubic scaling GW: Towards fast quasiparticle calculations. *Phys. Rev. B* **2016**, *94*, 165109.
- (120) Vidberg, H. J.; Serene, J. W. Solving the Eliashberg equations by means of N-point Padé approximants. *J. Low Temp. Phys.* **1977**, *29*, 179–192.
- (121) Armbruster, M. K.; Weigend, F.; Van Wüllen, C.; Klopper, W. Self-consistent treatment of spin-orbit interactions with efficient Hartree-Fock and density functional methods. *Phys. Chem. Chem. Phys.* **2008**, *10*, 1748–1756.

- (122) Desmarais, J. K.; Flament, J. P.; Erba, A. Spin-orbit coupling from a two-component self-consistent approach. I. Generalized Hartree-Fock theory. *J. Chem. Phys.* **2019**, *151*, 074107.
- (123) Förster, A.; Franchini, M.; van Lenthe, E.; Visscher, L. A Quadratic Pair Atomic Resolution of the Identity Based SOS-AO-MP2 Algorithm Using Slater Type Orbitals. *J. Chem. Theory Comput.* **2020**, *16*, 875 – 891.
- (124) Baerends, E.; Ziegler, T.; Atkins, A.; Autschbach, J.; Baseggio, O.; Bashford, D.; Bérces, A.; Bickelhaupt, F.; Bo, C.; Boerrigter, P.; Cavallo, L.; Daul, C.; Chong, D.; Chulhai, D.; Deng, L.; Dickson, R.; Dieterich, J.; Ellis, D.; van Faassen, M.; Fan, L.; Fischer, T.; Förster, A.; Guerra, C. F.; Franchini, M.; Ghysels, A.; Giammona, A.; van Gisbergen, S.; Goetz, A.; Götz, A.; Groeneveld, J.; Gritsenko, O.; Grüning, M.; Gusarov, S.; Harris, F.; van den Hoek, P.; Hu, Z.; Jacob, C.; Jacobsen, H.; Jensen, L.; Joubert, L.; Kaminski, J.; van Kessel, G.; König, C.; Kootstra, F.; Kovalenko, A.; Krykunov, M.; van Lenthe, E.; McCormack, D.; Michalak, A.; Mitoraj, M.; Morton, S.; Neugebauer, J.; Nicu, V.; Noodleman, L.; Osinga, V.; Patchkovskii, S.; Pavanello, M.; Peeples, C.; Philipsen, P.; Post, D.; Pye, C.; Ramanantoanina, H.; Ramos, P.; Ravenek, W.; Reimann, M.; Rodríguez, J.; Ros, P.; Rüger, R.; Schipper, P.; Schlüns, D.; van Schoot, H.; Schreckenbach, G.; Seldenthuis, J.; Seth, M.; Snijders, J.; Solà, M.; Stener, M.; Swart, M.; Swerhone, D.; Tognetti, V.; te Velde, G.; Vernooijs, P.; Versluis, L.; Visscher, L.; Visser, O.; Wang, F.; Wesolowski, T.; van Wezenbeek, E.; Wiesenekker, G.; Wolff, S.; Woo, T.; Yakovlev, A. ADF2022.1 (modified development version). 2022.
- (125) Rüger, R.; Franchini, M.; Trnka, T.; Yakovlev, A.; van Lenthe, E.; Philipsen, P.; van Vuren, T.; Klumpers, B.; Soini, T. AMS 2022.1, SCM, Theoretical Chemistry, Vrije Universiteit, Amsterdam, The Netherlands, <http://www.scm.com>. 2022.

- (126) Van Lenthe, E.; Baerends, E. J.; Snijders, J. G. Relativistic regular two-component hamiltonians. *J. Chem. Phys.* **1993**, *99*, 4597.
- (127) Van Lenthe, E.; Baerends, E. J.; Snijders, J. G. Relativistic total energy using regular approximations. *J. Chem. Phys.* **1994**, *101*, 9783–9792.
- (128) Van Lenthe, E.; Snijders, J. G.; Baerends, E. J. The zero-order regular approximation for relativistic effects: The effect of spin-orbit coupling in closed shell molecules. *J. Chem. Phys.* **1996**, *105*, 6505–6516.
- (129) Dyall, K. G. Interfacing relativistic and nonrelativistic methods. I. Normalized elimination of the small component in the modified Dirac equation. *J. Chem. Phys.* **1997**, *106*, 9618.
- (130) Kutzelnigg, W.; Liu, W. Quasirelativistic theory equivalent to fully relativistic theory. *J. Chem. Phys.* **2005**, *123*, 241102.
- (131) Dyall, K. G.; Dyana, K. G. An exact separation of the spin-free and spin-dependent terms of the Dirac–Coulomb–Breit Hamiltonian. *J. Chem. Phys.* **1994**, *100*, 2118.
- (132) Sadlej, A. J.; Snijders, J. G. Spin separation in the regular Hamiltonian approach to solutions of the Dirac equation. *Chem. Phys. Lett.* **1994**, *229*, 435–438.
- (133) Visscher, L.; Van Lenthe, E. On the distinction between scalar and spin–orbit relativistic effects. *Chem. Phys. Lett.* **1999**, *306*, 357–365.
- (134) Van Lenthe, E.; Baerends, E. J.; Snijders, J. G. Construction of the Foldy–Wouthuysen transformation and solution of the Dirac equation using large components only. *J. Chem. Phys.* **1996**, *105*, 2373.
- (135) Förster, A.; Visscher, L. GW100: A Slater-Type Orbital Perspective. *J. Chem. Theory Comput.* **2021**, *17*, 5080–5097.

- (136) Stuke, A.; Kunkel, C.; Golze, D.; Todorović, M.; Margraf, J. T.; Reuter, K.; Rinke, P.; Oberhofer, H. Atomic structures and orbital energies of 61,489 crystal-forming organic molecules. *Sci. Data* **2020**, *7*, 1–11.
- (137) Jensen, F. Atomic orbital basis sets. *Wiley Interdiscip. Rev. Comput. Mol. Sci.* **2013**, *3*, 273–295.
- (138) Te Velde, G.; Baerends, E. J. Precise density-functional method for periodic structures. *Phys. Rev. B* **1991**, *44*, 7888–7903.
- (139) Philipsen, P.; te Velde, G.; Baerends, E.; Berger, J.; de Boeij, P.; Franchini, M.; Groeneveld, J.; Kadantsev, E.; Klooster, R.; Kootstra, F.; Pols, M.; Romaniello, P.; Raupach, M.; Skachkov, D.; Snijders, J.; Verzijl, C.; Gil, J. C.; Thijssen, J. M.; Wiesenekker, G.; Peeples, C. A.; Schreckenbach, G.; Ziegler, T. BAND 2022.1 (modified development version), SCM, Theoretical Chemistry, Vrije Universiteit, Amsterdam, The Netherlands, <http://www.scm.com>. 2022.
- (140) Noro, T.; Sekiya, M.; Koga, T. Segmented contracted basis sets for atoms H through Xe: Sapporo-(DK)-nZP sets (n = D, T, Q). *Theor. Chem. Acc.* **2012**, *131*, 1–8.
- (141) Noro, T.; Sekiya, M.; Koga, T. Sapporo-(DKH3)-nZP (n = D, T, Q) sets for the sixth period s-, d-, and p-block atoms. *Theor. Chem. Acc.* **2013**, *132*, 1–5.
- (142) Becke, A. D. Density-functional thermochemistry. III. The role of exact exchange. *J. Chem. Phys.* **1993**, *98*, 5648–5652.
- (143) Bruneval, F.; Hamed, S. M.; Neaton, J. B. A systematic benchmark of the ab initio Bethe-Salpeter equation approach for low-lying optical excitations of small organic molecules. *J. Chem. Phys.* **2015**, *142*, 244101.
- (144) Kaltak, M.; Klimeš, J.; Kresse, G. Low scaling algorithms for the random phase ap-

- proximation: Imaginary time and laplace transformations. *J. Chem. Theory Comput.* **2014**, *10*, 2498–2507.
- (145) Kaltak, M.; Klimeš, J.; Kresse, G. Cubic scaling algorithm for the random phase approximation: Self-interstitials and vacancies in Si. *Phys. Rev. B* **2014**, *90*, 054115.
- (146) VÉril, M.; Romaniello, P.; Berger, J. A.; Loos, P. F. Unphysical Discontinuities in GW Methods. *J. Chem. Theory Comput.* **2018**, *14*, 5220–5228.
- (147) Monino, E.; Loos, P.-F. Unphysical Discontinuities, Intruder States and Regularization in GW Methods. *J. Chem. Phys.* **2022**, *231101*.
- (148) Pokhilko, P.; Yeh, C. N.; Zgid, D. Iterative subspace algorithms for finite-temperature solution of Dyson equation. *J. Chem. Phys.* **2022**, *156*, 094101.
- (149) In principle, there are 15 systems with multiple solutions. However, for Cl_4 , all three solutions are very close to each other. Therefore, we retain this system in our benchmark.
- (150) Bruneval, F. Ionization energy of atoms obtained from GW self-energy or from random phase approximation total energies. *J. Chem. Phys.* **2012**, *136*, 194107.
- (151) Bintrim, S. J.; Berkelbach, T. C. Full-frequency GW without frequency. *J. Chem. Phys.* **2021**, *154*, 041101.
- (152) Lebègue, S.; Arnaud, B.; Alouani, M.; Blochl, P. E. Implementation of an all-electron GW approximation based on the projector augmented wave method without plasmon pole approximation: Application to Si, SiC, AlAs, InAs, NaH, and KH. *Phys. Rev. B - Condens. Matter Mater. Phys.* **2003**, *67*, 155208.
- (153) Duchemin, I.; Blase, X. Robust Analytic-Continuation Approach to Many-Body GW Calculations. *J. Chem. Theory Comput.* **2020**, *16*, 1742–1756.

- (154) Kang, W.; Hybertsen, M. S. Quasiparticle and optical properties of rutile and anatase TiO₂. *Phys. Rev. B - Condens. Matter Mater. Phys.* **2010**, *82*, 085203.
- (155) Svane, A.; Christensen, N. E.; Gorczyca, I.; van Schilfgaarde, M.; Chantis, A. N.; Kotani, T. Quasiparticle self-consistent GW theory of III-V nitride semiconductors: Bands, gap bowing, and effective masses. *Phys. Rev. B - Condens. Matter Mater. Phys.* **2010**, *82*, 115102.
- (156) Punya, A.; Lambrecht, W.; van Schilfgaarde, M. Quasiparticle band structure of Zn-IV-N₂ compounds. *Phys. Rev. B - Condens. Matter Mater. Phys.* **2011**, *84*, 165204.
- (157) Tal, A.; Chen, W.; Pasquarello, A. Vertex function compliant with the Ward identity for quasiparticle self-consistent calculations beyond GW. *Phys. Rev. B* **2021**, *103*, 161104.
- (158) Cunningham, B.; Grüning, M.; Azarhoosh, P.; Pashov, D.; van Schilfgaarde, M. Effect of ladder diagrams on optical absorption spectra in a quasiparticle self-consistent GW framework. *Phys. Rev. Mater.* **2018**, *2*, 034603.
- (159) Cunningham, B.; Gruening, M.; Pashov, D.; van Schilfgaarde, M. QSGW: Quasiparticle Self consistent GW with ladder diagrams in W. *arXiv:2106.05759v1* **2021**,
- (160) Radha, S. K.; Lambrecht, W.; Cunningham, B.; Grüning, M.; Pashov, D.; van Schilfgaarde, M. Optical response and band structure of LiCoO₂ including electron-hole interaction effects. *Phys. Rev. B* **2021**, *104*, 115120.
- (161) Pyykko, P.; Desclaux, J. P. Relativity and the Periodic System of Elements. *Acc. Chem. Res.* **1979**, *12*, 276–281.
- (162) Marie, A.; Loos, P.-F. A similarity renormalization group approach to Green's function methods. *arXiv:2303.05984* **2023**, 1–14.

- (163) Friedrich, C. Tetrahedron integration method for strongly varying functions: Application to the GT self-energy. *Phys. Rev. B* **2019**, *100*, 075142.
- (164) Pollehn, T. J.; Schindlmayr, A.; Godby, R. W. Assessment of the GW approximation using Hubbard chains. *J. Phys. Condens. Matter* **1998**, *1*, 1273.
- (165) Vlček, V.; Baer, R.; Rabani, E.; Neuhauser, D. Simple eigenvalue-self-consistent \$GW_0\$. *J. Chem. Phys.* **2018**, *149*, 174107.
- (166) Samanta, P. K.; Kim, D.; Coropceanu, V.; Brédas, J. L. Up-Conversion Intersystem Crossing Rates in Organic Emitters for Thermally Activated Delayed Fluorescence: Impact of the Nature of Singlet vs Triplet Excited States. *J. Am. Chem. Soc.* **2017**, *139*, 4042–4051.

Graphical TOC Entry

